Particle Physics at CERN

Annual Report 2011

(SNF grants 200020_134620 and 206620_134610)

E. Aguiló, Y. Allkofer, C. Amsler, A. Benelli, C. Canali, W. Creus, S. de Visscher, A. Ferella, M. Ivova Rikova, L. Jørgensen, M. Kimura, R. Medard, B. Millán Mejías, P. Otyugova, C. Regenfus, P. Robmann, J. Rochet, A. Schmidt, J. Storey, and M. Walter.

V. Chiochia, C. Favaro, H. Snoek, S. Tupputi, and M. Verzetti.

April 18, 2012

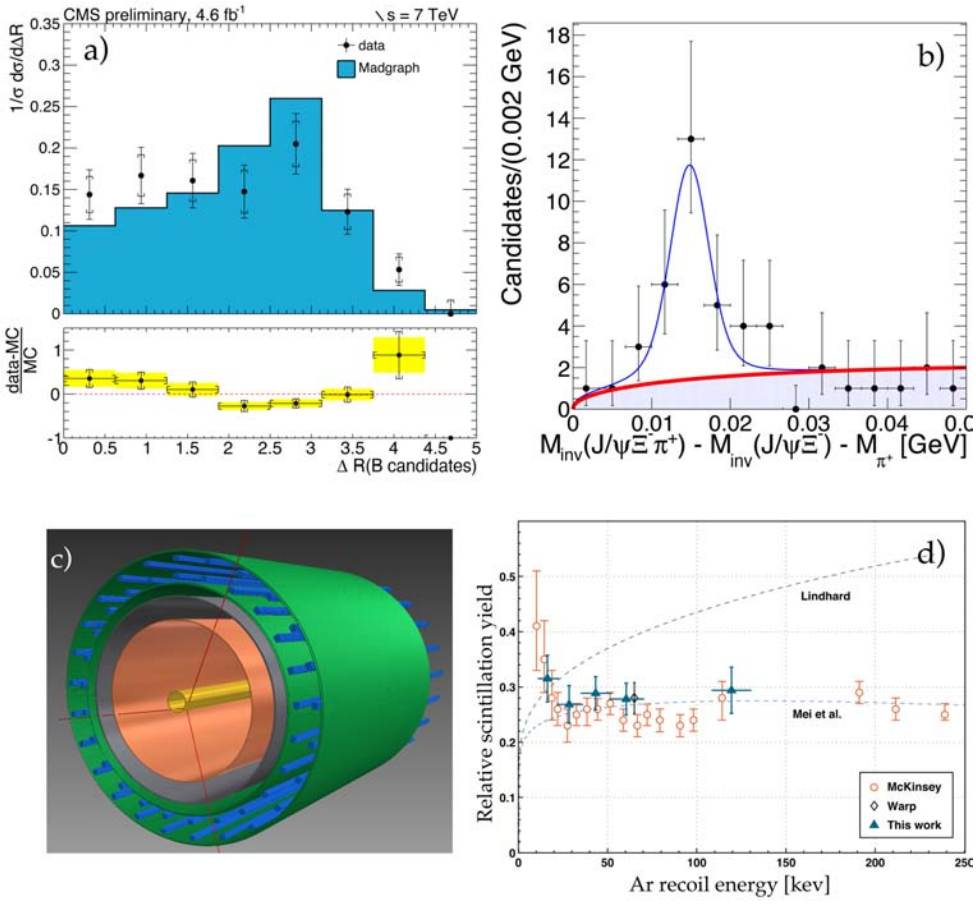

Physik-Institut der Universität Zürich
Winterthurerstrasse 190, CH-8057 Zürich, Switzerland

Contents

This report covers the activities of the Zürich group at CERN on the CMS, AEgIS, DARWIN and DIRAC projects between 1 April 2011 and 31 March 2012. It does not include the activity of one of us (C. A.) contributing to the "Review of Particle Physics" (Particle Data Group). Further details and publication reprints can be obtained from our home page, see http://cern.ch/unizh/.

Cover picture:
a) Normalized cross section for $Z^0 b\bar{b}$ production at 7 TeV and Monte Carlo simulation (aMC@NLO); b) Q-value distribution of $\Xi_b^- \pi^+ \rightarrow J/\psi\ \Xi^- \pi^+$ with Ξ_b^{*0}-signal; c) Fast Annihilation Tracking (FACT) scintillation fiber detector for AEgIS; d) Light yield in liquid argon as a function of recoil energy.

1 Particle physics with CMS

E. Aguiló, C. Amsler, S. de Visscher, M. Ivova, B. Millán Mejías, P. Otyugova,
M. Rebero‡, P. Robmann, and A. Schmidt,

V. Chiochia, C. Favaro, H. Snoek, S. Tupputi, and M. Verzetti

In collaboration with the CMS Collaboration
‡ CERN summer student

In 2011 the Large Hadron Collider delivered an integrated luminosity of 5.7 fb^{-1} at 7 TeV (fig. 1.1) while at most 1 fb^{-1} had been expected at the beginning of the run operation back in March. During this long run CMS recorded 5.2 fb^{-1} of data with its subdetectors performing at an efficiency of 98.5%. The silicon barrel pixel detector, the innermost component of the CMS experiment ,was developed in and commissioned by our group (in collaboration with PSI). It allows a precise reconstruction of charged particle tracks and the identification of secondary vertices from long-lived particles. This device is crucial for our research using b-quarks. Details can be found in earlier annual reports.

More than one hundred refereed journal articles have been published by the CMS collaboration in 2011. One of us (V. C.) co-chaired the B-physics analysis group, that has so far released twelve journal articles on quarkonium, B hadron decays and b-quark production measurements. H. S. convened the pixel calibration and reconstruction group, S. d.V. coordinated the simulation in the standard model (SM) physics group. Here we report on the analysis results achieved by the Zurich group on heavy baryons, B_s decays, Higgs searches in τ-lepton pairs and $b\bar{b}$ angular correlations.

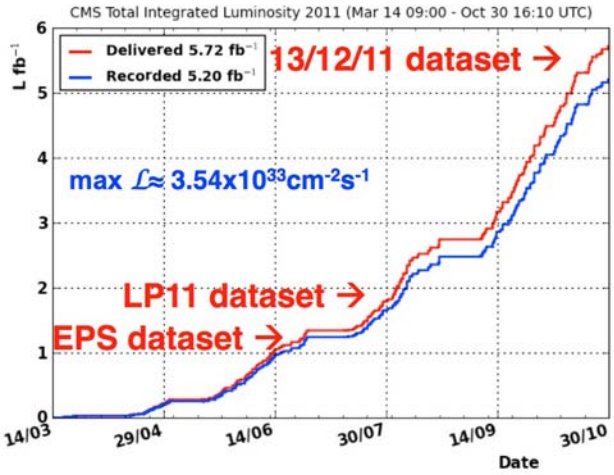

Figure 1.1: *Integrated luminosity in the 2011 LHC run at $\sqrt{s}$ = 7 TeV.*

1.1 Study of Λ_b and Σ_b

The spectroscopy of b-baryons provides valuable information to test QCD models. Baryon production mechanisms and dynamics of heavy quark decay can be studied from polarization measurements in b-baryon decays. Our group is studying the Λ_b polarization in the decay $\Lambda_b \to J/\psi\,(\to \mu^+\mu^-)\Lambda(\to p\pi^-)$ (fig. 1.2, left). To select clean Λ_b candidates large transverse momenta and narrow windows around the Λ and J/ψ masses are chosen, and tight vertex cuts chosen for the daughter particles. The

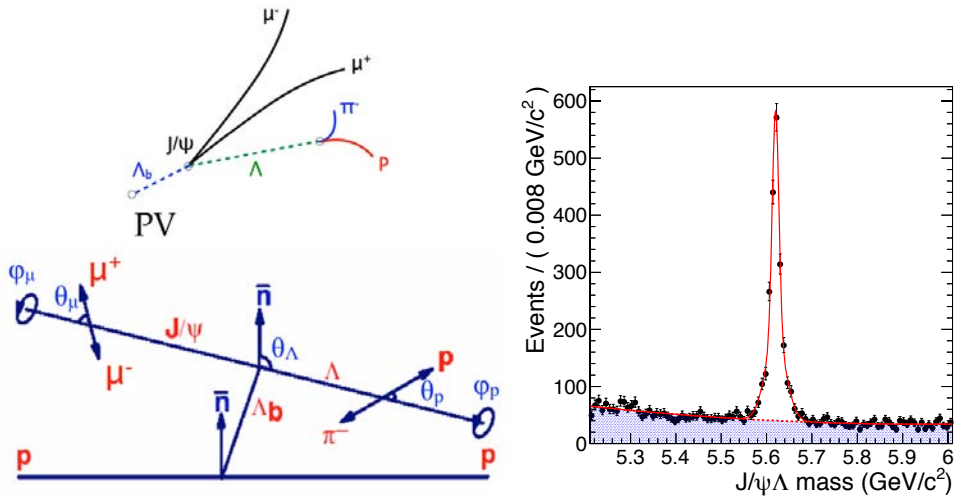

Figure 1.2: *: Left: Decay* $\Lambda_b \to J/\psi\ (\to \mu^+\mu^-)\Lambda(\to p\pi^-)$ *and angles used in the* Λ_b *polarization analysis. Right:* $J/\psi\ \Lambda$ *invariant mass distribution with* Λ_b *fit (red line).*

$J/\psi\ \Lambda$ invariant mass distribution is shown in fig.1.2 (right) from 5 fb^{-1} of integrated luminosity, leading to 1929 ± 54 Λ_b-baryons.

We use the angles θ_Λ, θ_p and θ_μ, the polar angles of the Λ, the proton and the μ^+ in the respective rest frames of Λ_b, Λ and J/ψ (fig.1.2, left). The Λ_b polarization manifests itself by a slope in the $\cos\theta_\Lambda$ distribution that can be extracted by analyzing the angular correlations between the daughter particles [1]. The distortions in the angular distributions due to acceptance and cuts are taken into account by Monte Carlo simulation. Sidebands of the Λ_b mass peak are used to estimate the contamination from background. A maximum likelihood fit is then performed. Figure 1.3 shows for instance a preliminary distribution of cosθ_p and cosθ_μ together with fits. Work on this analysis is in progress [2].

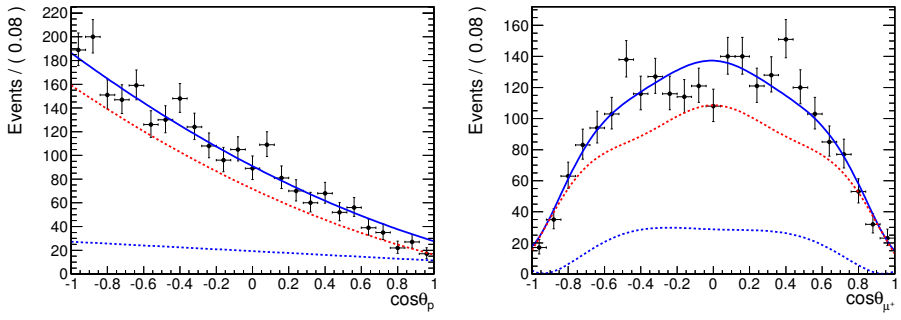

Figure 1.3: *:* $\cos\theta_p$ *(left) and* $\cos\theta_\mu$ *(right) distributions in the* Λ *and* J/ψ *rest frames, respectively, with the results of a multidimensional likelihood fit (blue line). The dashed lines show the fits to the* Λ_b *signal (red) and the background contribution (blue).*

The Λ_b candidates are also used to reconstruct the four states $\Sigma_b^{(*)\pm} \to \Lambda_b\pi^\pm$ where the Σ_b or Σ_b^* decays strongly at the primary vertex. Tight requirements are applied on the soft pion to suppress the

large combinatorial background from other tracks. Figure 1.4 shows the distributions of the Q-values of the decays. The reconstructed candidates can be used to measure Σ_b cross-sections relative to those for Λ_b.

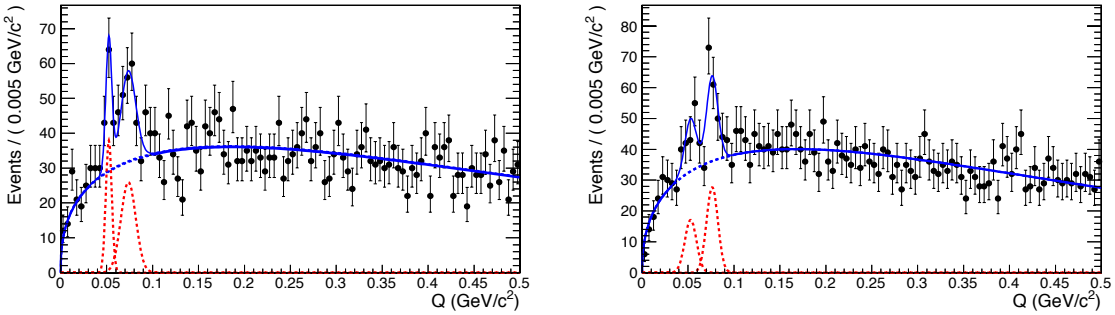

Figure 1.4: *Q-value distributions for the* $\Sigma_b^{(*)}$ *decays, where* $Q = M(\Lambda_b\pi) - M(\Lambda_b) - M(\pi)$. *Left:* Σ_b^+ *and* Σ_b^{*+}. *Right:* Σ_b^- *and* Σ_b^{*-}.

1.2 Observation of a new strange bottom baryon

The $\Xi_b^-(5790)$, a dbs-baryon, and its Ξ_b^0 isospin partner, a ubs-baryon, have been observed at the Tevatron [3]. However, there are two other ground state pairs of baryons in the SU(4) classification, the Ξ_b' with spin 1/2 and the Ξ_b^* with spin 3/2, which can both be negatively charged (dsb) or neutral (usb). Theory (e.g. ref. [4]) predicts the mass difference between the Ξ_b' and the Ξ_b to be smaller than the mass of the pion, which forbids the decay $\Xi_b' \to \Xi_b\pi$. In contrast, the Ξ_b^* would be heavy enough to decay (strongly) into the Ξ_b by pion emission.

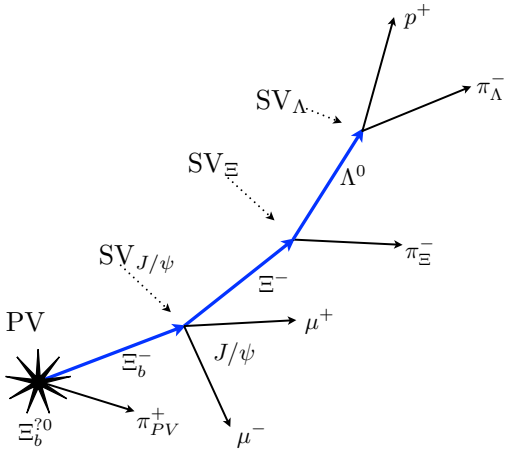

Figure 1.5: *Decay chain of the new baryon (marked* $\Xi^{?0}$ *at the primary vertex PV). Charge conjugation (baryons and antibaryons) is implicitely assumed.*

We have observed a new usb-baryon decaying into $\Xi_b^-\pi^+$ using 5.0 fb^{-1} of data. We reconstruct the decay $\Xi_b^- \to J/\psi\,\Xi^-$, with $J/\psi \to \mu^+\mu^-$ and $\Xi^- \to \Lambda\pi^-$, $\Lambda \to \pi^- p$ (fig. 1.5). The events were collected with a trigger requiring a secondary vertex (SV) displaced from the primary (PV), from which two muons emerge with transverse momenta larger than 3 GeV/c and invariant mass compatible with the J/ψ (for details on additional selection cuts see ref. [5]). The Λ (or $\overline{\Lambda}$) decays into two opposite charges. The higher momentum track is assumed to be the proton. The two tracks are required to form a vertex displaced from the beamline. The candidate Ξ^- (or $\overline{\Xi^-}$) is reconstructed

by combining the Λ with an additional track. A kinematic vertex fit is performed in which the track is assumed to be a pion and the Λ mass constrained to its known value. Figure 1.6 (left) shows the $\Lambda\pi^-$ invariant mass distribution with the Ξ^- signal. The Ξ^-s are then combined with the J/ψ with a kinematic vertex fit, constraining the Ξ^-- and J/ψ-masses to their known values. The resulting $J/\psi\ \Xi^-$ invariant mass distribution with the Ξ_b^- peak (108 $\pm$ 14 events) is displayed in fig. 1.6 (middle) after all selection cuts. The measured mass is in good agreement with the known value.

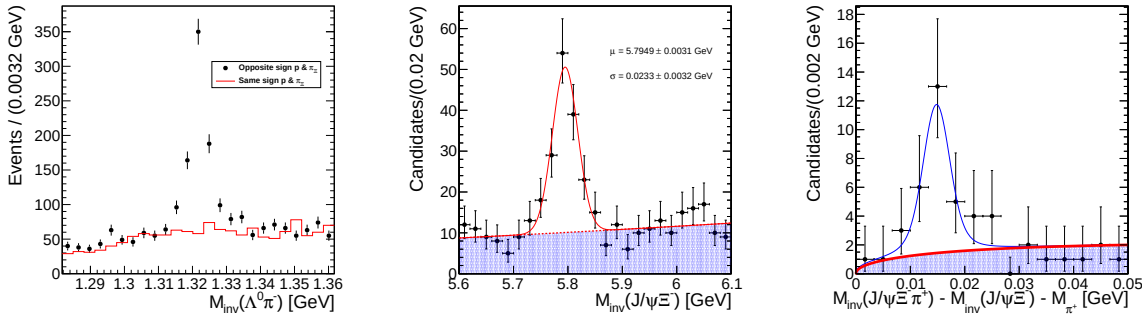

Figure 1.6: *Left: $\Lambda\pi^-$ invariant mass distribution showing the Ξ^-. Middle: $J/\psi\ \Xi^-$ invariant mass distribution showing the Ξ_b^- signal with fit. Right: Q-value distribution of the reaction $\Xi_b^-\pi^+ \rightarrow J/\psi\ \Xi^-\pi^+$ showing the new Ξ_b^{*0} with fits.*

We then combine the Ξ_b^- baryon with an additional track assumed to be a π and emerging from the PV with charge opposite to the π from Ξ^- (or $\overline{\Xi^-}$) decay, and search for narrow resonances in the mass difference distribution (fig. 1.6, right). We observe 29 candidates (with a background of 6.6 $\pm$ 2.6) and obtain a mass of 5944.9 $\pm$ 2.8 MeV. This state is thus 154 MeV heavier than the spin 1/2 Ξ_b^-. Unfortunately the data sample is too small to determine its spin from the decay angular distributions. According to predictions this new baryon would be the Ξ_b^{*0} with spin 3/2.

1.3 Lifetime of the B_s-meson

We are measuring the width difference $\Delta\Gamma_s = \Gamma_L - \Gamma_H$ of the two CP-Eigenstates of the B_s-meson, B_L (CP = +1) and B_H (CP = -1) in the decay $B_s \rightarrow J/\psi\ (\rightarrow \mu^+\mu^-)\ \phi(\rightarrow K^+K^-)$. Three angles are needed to describe this decay. The angles θ and ϕ give the flight direction of the μ^+ in the J/ψ rest frame while ψ is the azimuthal angle of the K^+ with respect to the flight direction of the J/ψ. Since the B_s is pseudoscalar, while the J/ψ and ϕ are vectors, the angular momentum between the two decay products is L = 0, or 2 for B_L and L = 1 for B_H. Hence the angular distributions are different for the two states (for details see e.g. ref. [6]).

During 2011 we collected 15'000 $B_s \rightarrow J/\psi(\rightarrow \mu^+\mu^-)\phi(\rightarrow K^+K^-)$ events at $\sqrt{s} = 7$ TeV with an integrated luminosity of 4.6 fb^{-1}. Our B_s are "untagged", which means that we do not distinguish between B_s and $\overline{B}_s$. The muons pairs are selected with a trigger on displaced J/ψ decay point with respect to the primary vertex. Various cuts are applied, in particular the muons and kaons are required to have transverse momenta larger than 4, respectively 0.7 GeV/c. An additional cut on the decay length reduces the prompt J/ψ background from the primary vertex. The $B_s \rightarrow J/\psi\ \phi$ peak is shown in fig. 1.7.

Side band subtraction is applied to determine the contribution from background. Efficiency and acceptance corrections are calculated by Monte Carlo simulation. The results of the likelihood fit taking into account the mass, decay length and angular distributions are shown in fig. 1.8. The

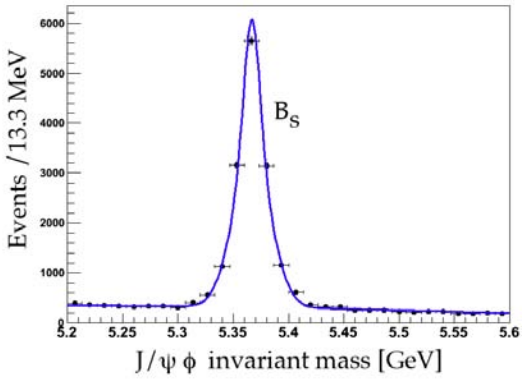

Figure 1.7: *J/ψ ϕ invariant mass showing the B_s (15'000 events).*

dark blue line is the fit, the dotted blue (magenta) line is the contribution from the CP even (odd) component. Fitted mass and mean life are in excellent agreement with the known values (5366 MeV and 1.43 ps). This work is still in progress [7] and we obtain a preliminary value for $\frac{\Delta\Gamma_s}{\Gamma_s}$ of 0.107 $\pm$ 0.019, where the error is statistical only. This is compatible with the prediction from the SM: 0.147 $\pm$ 0.060.

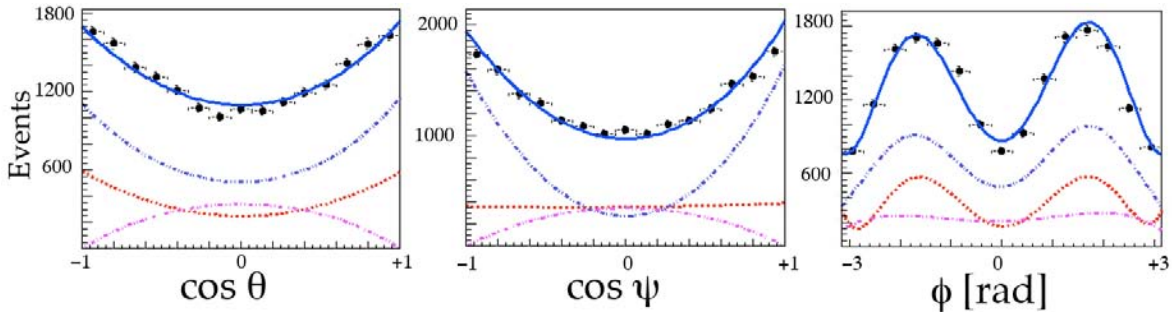

Figure 1.8: *Measured angular distributions. The dark blue line is the fit, the dotted blue line is the CP-even component, the magenta line the CP-odd component. The red curve shows the background contribution.*

1.4 Searches for the Higgs boson in $\tau^+\tau^-$ decays

An important goal of the LHC physics program is to ascertain the mechanism of electroweak symmetry breaking, through which the W and Z^0 bosons obtain mass, while the photon remains massless. In the SM this is achieved via the Higgs mechanism which predicts the existence of a scalar Higgs boson. The minimal supersymmetric standard model (MSSM) contains two Higgs doublets, giving rise to five physical states: a light neutral CP-even state (h), a heavy neutral CP-event state (H), a neutral CP-odd state (A), and a pair of charged states ($H^{\pm}$).

A search for the neutral Higgs boson decaying into τ-pairs was performed using an integrated luminosity of 4.6 fb^{-1} [8]. Three independent τ-pair final states were studied with one (or both) τ-leptons decaying leptonically. The distribution of the τ-pair invariant mass for all channels combined is shown in fig. 1.9 (left) for the MSSM search. The spectra show no evidence for a Higgs boson in both MSSM and SM searches. Upper bounds (95% CL) on the Higgs boson cross section times the branching fraction into τ-pairs are shown in fig. 1.9 (right). We exclude a Higgs boson with mass

$m_H = 125$ GeV with a production cross section 4.4 times that predicted by the SM. The MSSM search excludes previously unexplored regions of the parameter space, reaching as low as $\tan\beta = 7.1$ at $m_A = 160$ GeV.

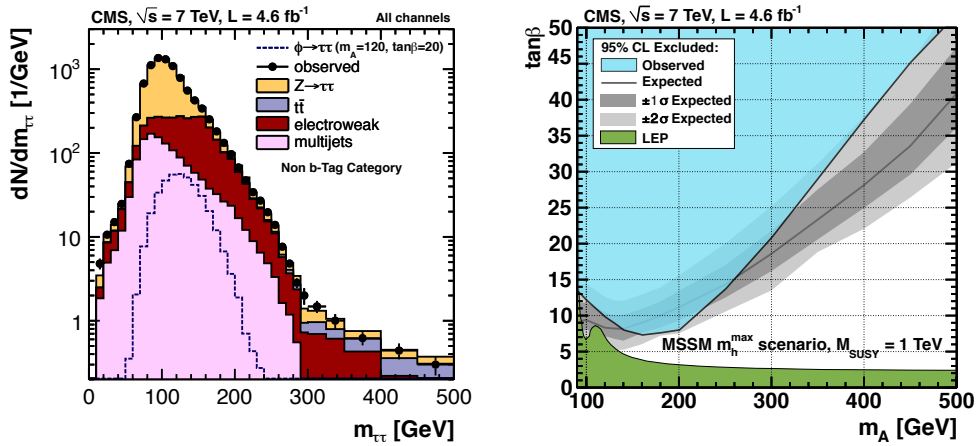

Figure 1.9: *Left: τ-pair invariant mass distribution in the MSSM Higgs boson search for data (full dots) and simulation (stacked histograms). Right: Region in the $\tan\beta$ vs. m_A parameter space excluded at 95% CL in the MSSM m_h^{max} scenario.*

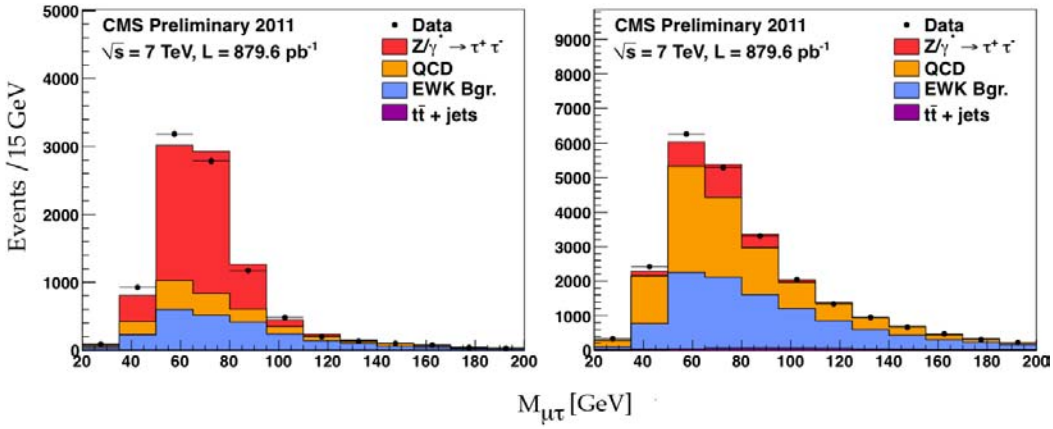

Figure 1.10: *τ-pair invariant mass distribution with various signal and background processes for events passing the identification cut (left) and for those failing the identification cut (right).*

These Higgs searches rely on the precise estimate of the reconstruction efficiency for the τ hadronic decay, which was measured by our group using a *tag-and-probe* technique [9]. This method exploits the decay $Z^0 \to \tau_\mu \tau_{\rm had}$, where τ_μ is a τ decaying into a μ while $\tau_{\rm had}$ represents a τ decay into charged hadrons. The events are required to have exactly one isolated μ and a jet of opposite sign. The events are divided into those surviving a tight cut and those failing the cut, and a simultaneous fit of the visible τ-pair invariant mass is performed in the signal and background regions (fig. 1.10). The measured τ identification efficiency is typically 60% and agrees well with Monte Carlo simulation.

The overall precision of the measurement is 6% (including systematic errors). With the higher instantaneous luminosity in 2012 we will further quantify the performance of hadronic τ reconstruction in an environment characterized by a larger number of simultaneous pp collisions. We are also responsible for the development of the software monitoring the performance of τ-lepton identification.

1.5 Improvements to the pixel hit reconstruction

We are developing a novel hit reconstruction technique to improve the spatial disentanglement in a dense charged track environment. The implementation of this technique in the CMS software will affect all analyses that depend on the reconstruction of high energetic jets, such as b or τ jets. A fraction of 65% of the τ decay hadronically. The transverse momentum of the τ being large compared to its mass, the tracks in the jet are close to each other. Therefore, excellent spatial resolution is needed for τ reconstruction.

A significant amount of the hadronic τ decays are produced in three charged tracks accompanied by the (invisible) neutrino. The higher the τ momentum, the more collimated the three tracks, which makes them at some point inseparable. In the innermost pixel layer this effect starts to occur for opening angles between the two trajectories of about 5 mrad. For a typical 3-prong τ decay this corresponds to a transverse momentum of 150 GeV/c. The merging of clusters deteriorates the measurement of the particle trajectories and the reconstruction of the τ-lepton.

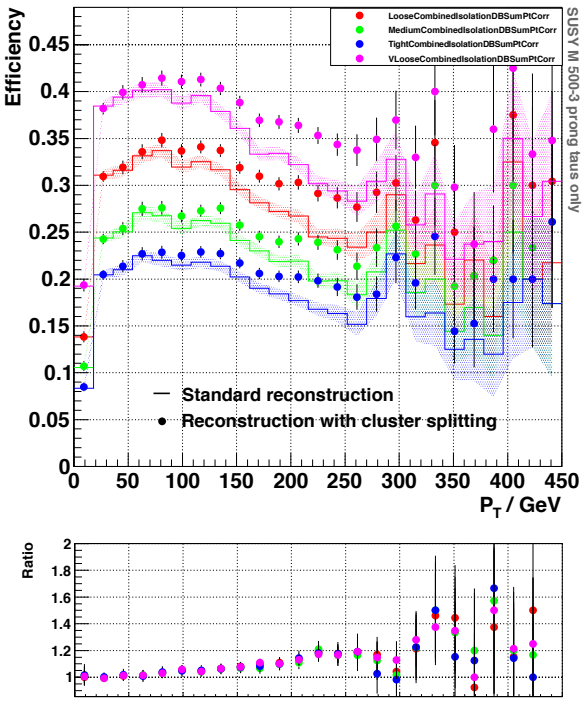

Figure 1.11: *τ identification efficiency as a function of transverse momentum for Higgs decays. The dots show the improved hit reconstruction based on pixel hit splitting compared to the standard case (histograms). The colors represent the various τ identification procedures. The lower plot shows the relative improvement.*

The charge measured for each cluster, together with an estimate of the track impact angle, can be used to discriminate merged clusters from isolated clusters. We have developed an algorithm for splitting merged pixel clusters, now deployed in the CMS software. The performance improvement in the τ reconstruction was verified on a simulated sample of 500 GeV MSSM Higgs bosons decaying into τ-pairs. Figure 1.11 shows the τ identification efficiency for 3-prong decays as function of τ transverse momentum. Our algorithm improves the identification efficiency by $\sim$20% for $p_T(\tau) >$

200 GeV/c for the four τ identification procedures in CMS (fig. 1.11, bottom).

1.6 Studies of B hadron correlations associated to Z^0 bosons

A measurement of the b-quark production associated with a Z^0/γ^* is an important test of QCD and is of great experimental relevance for various searches. The process constitutes a background to the SM Higgs production decaying to $b\bar{b}$, associated with vector bosons. In addition, in models with extended Higgs sector (such as the two-Higgs doublet models), a discovery channel would be $\phi_1 \rightarrow Z^0\phi_2$ with $\phi_2 \rightarrow \mathrm{b\bar{b}}$, where $\phi_{1,2}$ are neutral Higgs bosons. Finally, the description of the b-quark dynamics remains difficult, in particular in the soft-collinear region, where the gluon splitting contribution to $q\bar{q}$-pairs is not well known.

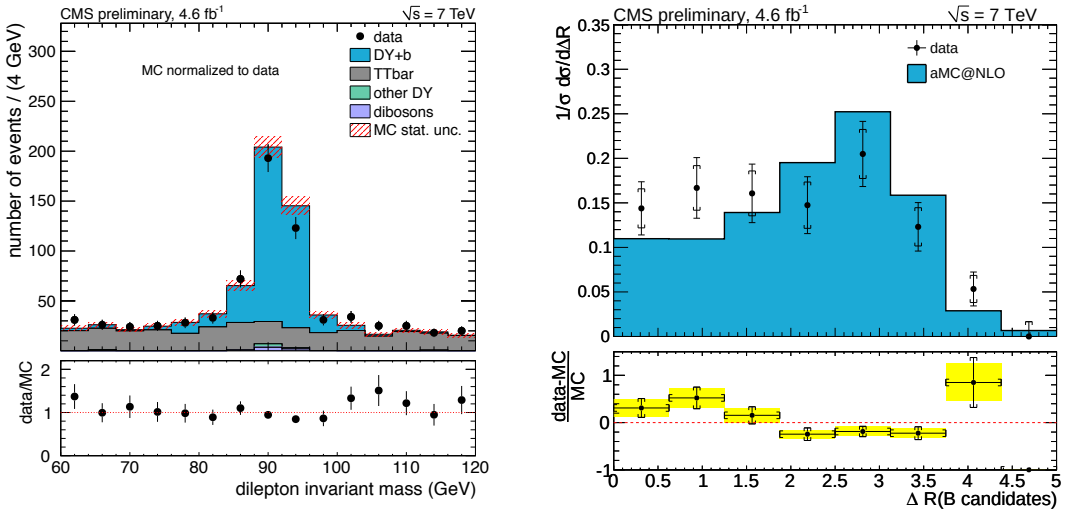

Figure 1.12: *Left: Dilepton invariant mass distribution. Right: Normalized production cross section as a function of the angular variable* $\Delta R = \sqrt{\Delta\eta^2 + \Delta\phi^2}$. *The measured distribution (solid dots) is compared to* `aMC@NLO` *prediction.*

Our group has performed a measurement of the normalized differential cross-section $pp \rightarrow Z^0/\gamma^* + b\bar{b}$ as a function of B-hadron angular separation [10] for an integrated luminosity of 4.6 fb^{-1}. Leptonic decays of the Z^0 into two leptons (e or μ) of opposite charges are selected (fig. 1.12, left). The B-hadron pairs are identified by the Inclusive Vertex Finder (IVF) algorithm, based on the reconstruction of displaced secondary vertices from B decays, independently from jets. This allows to resolve B-hadron pairs even at small opening angles (see fig. 1.13) for which decay products merge into single jets, the standard b-jet tagging techniques then becoming useless.

The observed distribution is compared to the the NLO expectation obtained with `aMC@NLO` (fig. 1.12, right). The data agree reasonably well with simulation within experimental errors, although data suggest a flatter angular distribution at small ΔR. Additional investigations and larger data samples in 2012 will help establishing which theoretical model provides the best description of the data [11].

We are also working on the implementation of the jet matching techniques for the `MADGRAPH` Monte Carlo simulation which will allow to efficiently produce exclusive samples of $pp \rightarrow Z^0/\gamma^* + b\bar{b}$ events with additional partons. We are implementing the simulation of massive b-quarks in `MADGRAPH`.

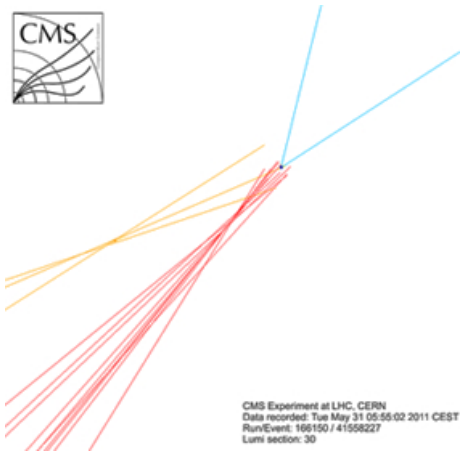

Figure 1.13: *Event with two displaced vertices from B-hadron decays (red and yellow tracks) and two leptons from a Z^0 boson (blue tracks).*

Our group has furthermore improved the b-jet identification in the High Level Trigger (HLT). The reconstruction of the primary vertex is crucial for the application of b-tagging algorithms. To limit CPU time the standard HLT reconstruction performs only a fast 1D estimate of the primary vertex position in the direction of the beam axis, while the coordinates of the online beam spot are used as estimates for the transverse vertex position. The efficiency of the trigger can be improved with an event-by-event estimate of the 3D vertex position at the trigger level. We have assessed the performance of the 3D primary vertex reconstruction using a simulated sample of jet events and an average event pileup of 10, and have established that the algorithm can be successfully applied at trigger level.

References

[1] M. Kramer and H. Simma, Nucl. Phys. **B 50** (1996) 125
[2] M. Ivova Rikova, PhD-thesis, Universität Zürich (in preparation)
[3] V. M. Abazov *et al.*, Phys. Rev. Lett. **99** (2007) 052001;
T. Aaltonen *et al.*, Phys. Rev. Lett. **99** (2007) 052002
[4] M. Karliner *et al.*, arXiv:0706.2163 [hep-ph] (2007)
[5] E. Aguiló, CMS-PAS-BPH-12-001 (to be published)
[6] L. Wilke, PhD-Thesis, University of Zurich (2009)
[7] B. Millán Mejías, PhD-thesis, Universität Zürich (in preparation)
[8] CMS Collaboration, submitted to Phys. Lett. B, prep. arXiv:1202.4083 [hep-ex] (2012)
[9] M. Verzetti, PoS (EPS-HEP2011) 417 (2011)
[10] CMS Collaboration, CMS-PAS-EWK-11-015 (to be published)
[11] C. Favaro, PhD-thesis, Universität Zürich (in preparation)

2 Test ot the equivalence principle with antihydrogen

Y. Allkofer, C. Amsler, C. Canali, L. Jørgensen, M. Kimura, C. Regenfus, J. Rochet, and J. Storey

In collaboration with:
INFN Bescia - Firenze - Genova - Milano - Padova - Pavia - Trento, CERN, MPI-K (Heidelberg), Kirchoff Inst. of Phys (Heidelberg), INR (Moscow), ITEP (Moscow), Univ. Claude Bernard (Lyon), Univ. of Oslo, Univ. of Bergen, Czech Tech. Univ (Prague), ETH-Zurich, Politecnico Milano, Laboratoire Aimé Cotton (Orsay).

(AEgIS Collaboration)

The AEgIS experiment [1] will measure for the first time the gravitational acceleration of antimatter $\bar{g}$ using a beam of antihydrogen ($\bar{H}$) atoms. Previous attempts to measure $\bar{g}$ with positrons and antiprotons failed due to stray electric or magnetic fields. From attempts to unify gravity with the other forces the possibility that $\bar{g} \neq g = 9.81$ m s^{-2} cannot be excluded [2]. Many arguments have been put forward to rule out any difference between g and $\bar{g}$, and correspondingly many rebuttals have been published [3]. The validity of the weak equivalence principle (WEP) for antimatter thus rests on experimental evidence.

The goal of AEgIS is to measure $\bar{g}$ with an initial precision of 1%. First we need to produce $\bar{H}$-atoms at $\sim$100 mK. A promising technique [4] uses the interaction between the antiproton and the highly excited Rydberg state positronium (Ps*) in which the bound positron is captured by the antiproton and an electron is released ($\mathrm{Ps}^* + \bar{\mathrm{p}} \rightarrow \overline{\mathrm{H}}^* + \mathrm{e}^-$). Fig. 2.14 shows a sketch of the apparatus. The process begins with the production of positronium (Ps) by accelerating 10^8 positrons from a Surko type accumulator onto a nanoporous material. The ortho-Ps emitted from the target is then brought to the Rydberg state Ps* by two-step laser excitation. Some of the Ps* atoms diffuse across a Penning trap in which 10^5 antiprotons from the CERN antiproton decelerator (AD) have been stored, producing $\bar{H}$ through the charge exchange reaction.

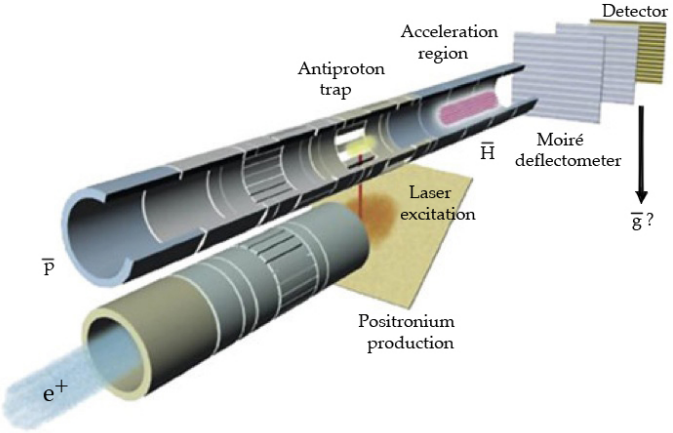

Figure 2.14: *Sketch of the AEGIS apparatus. The $\bar{H}$-atoms are produced in the $\bar{p}$-trap in a 1T field. Not shown are $\bar{p}$- and e^+-capture traps in the 5T magnet at the entrance of the apparatus.*

An electric field is then applied along the beam axis to accelerate the $\bar{H}$-atoms to $\sim$400 m/s. This technique has already been demonstrated by members of the AEgIS collaboration with hydrogen atoms [5]. A Moiré deflectometer consisting of two gratings and a position sensitive annihilation detector is used to measure the deflection of the $\bar{H}$ beam in the gravitational field. The downward (or upward!) shift of the Moiré intensity pattern at the detector due to gravity needs to be combined with time-of-flight and be measured with a vertical precision of $\sigma \simeq 10$ μm. The Zürich group is designing

and building (i) the annihilation detector and its readout to characterize the $\bar{p}/\bar{H}$ cloud in the Penning trap and (ii) the position sensitive detector to measure the Moiré pattern.

The AEgIS apparatus, less the Moiré deflectometer, will be installed for the AD runs in 2012. Objectives are to produce $\bar{H}$-atoms, measure their temperature and demonstrate the production of the $\bar{H}$-beam by means of Stark acceleration. The goal of our group is to commission the Fast Annihilation Cryogenic Tracking (FACT) detector designed and constructed in 2011/2012.

Depending on temperature, a large fraction of the $\bar{H}$-atoms annihilate by hitting the confinement walls within $\sim\mu$s. The detector must therefore be very fast, but only needs to be active for 1 ms every 100 s between AD pulses. The operating conditions are challenging as the detector occupies a cylindrical volume around the trap with an inner radius of 78 mm and outer radius of 103 mm in a 1T magnetic field, and must operate at 4K. A further complication is the strong 511 keV γ background produced by positrons hitting the positronium target. This occurs a few μs before the first $\bar{H}$ annihilations.

We have opted for a scintillating fiber detector with silicon photomuliplier readout. The FACT detector consists of four layers of 1 mm diameter scintillating fibers[1] coupled to clear fibers of the same diameter which direct the optical signal from the cryogenic region onto arrays of 1 mm diameter silicon photomultipliers (MPPC)[2]. Each layer consists of 200 scintillating fiber loops aligned orthogonal to the beam axis. A sketch is shown in fig. 2.15. A vertex resolution along the longitudinal axis of 2.5 mm is expected from simulations, which is sufficient for our requirements.

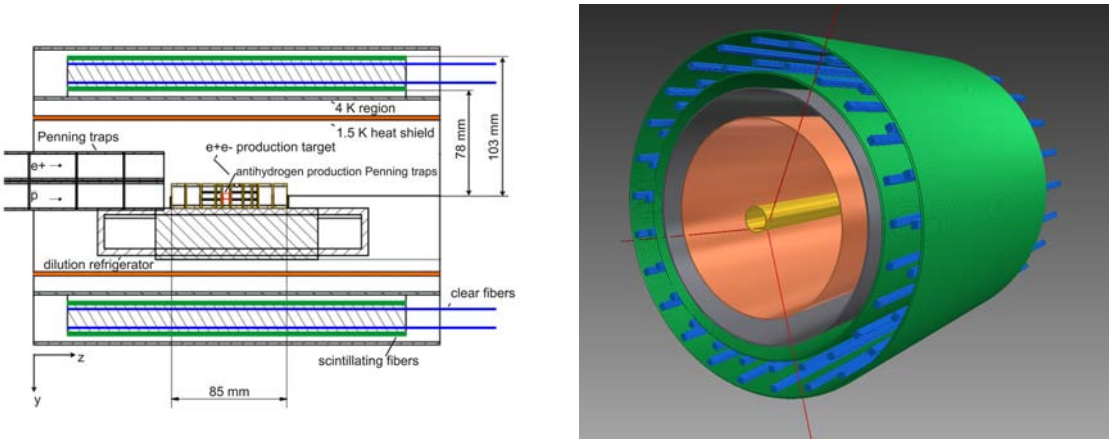

Figure 2.15: *Conceptual design of the Fast Annihilation Tracking (FACT) detector (see text).*

The readout electronics for the 800 fibers must be fast enough to measure the speed (temperature) of the $\bar{H}$-atoms. The output of the MPPCs is sampled continuously. The principle is shown in the bottom part of fig. 2.16 (left) for a single channel. The MPPC is connected to a linear amplifier and a fast discriminator feeding the FPGA. The latter controls the MPPC voltage and threshold levels, samples the output of the comparators with a time resolution of $\sim$10 ns, and transfers the data to the DAQ system through a USB connection. A single FPGA manages several channels (upper part of fig. 2.16, left). The FPGA can be programmed to perform a fast and smart real time readout of all channels. The MPPCs are located inside and the readout electronics outside the AEgIS apparatus (fig.2.16, right).

The scintillating fibers must operate at 4K. Since no data exist we have tested the performance

[1] Kuraray SCSF-78M multi-clad scintillating fibers [6].

[2] Hamamatsu silicon photomultipliers MPPC S10362-11-100C [7].

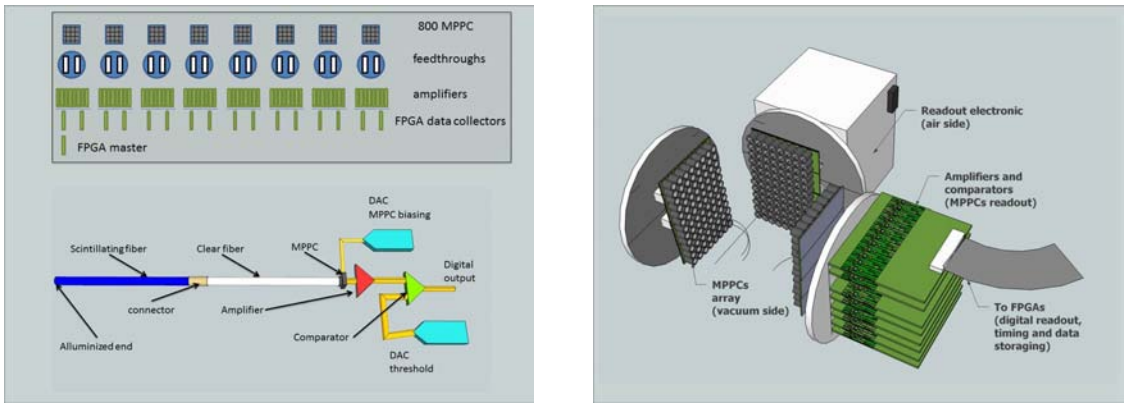

Figure 2.16: *Left: electronics layout for the fiber readout (see text) and readout for one scintillating fiber. Right: MPPCs inside the vacuum region connected by feedthroughs to the readout electronics.*

of scintillating fibers with cosmic rays at cryogenic temperatures. The test apparatus consisted of 3 layers of 1 mm diameter Kuraray scintillating fibers arranged in loops at the bottom of a liquid helium cryostat (fig.2.17, left). The light from the scintillating fibers was detected by 3 MPPCs, the outputs of which were amplified and digitized by a LeCroy Wavepro 7100 10 GS/s oscilloscope. The oscilloscope was triggered when the signal of two of the three fibers exceeded 4 photoelectrons and we counted events with a coincidence observed in the third fiber, corresponding to the passage of a cosmic ray through the three fiber layers. The cryostat was filled with liquid helium immersing the fibers for 4 hours during which the detection efficiency was monitored, followed by warm-up to ambient temperature. The rate of events as a function of temperature is shown in fig.2.17 (right). We observed a small ($\sim$15%) decrease in light yield from room to liquid helium temperature.

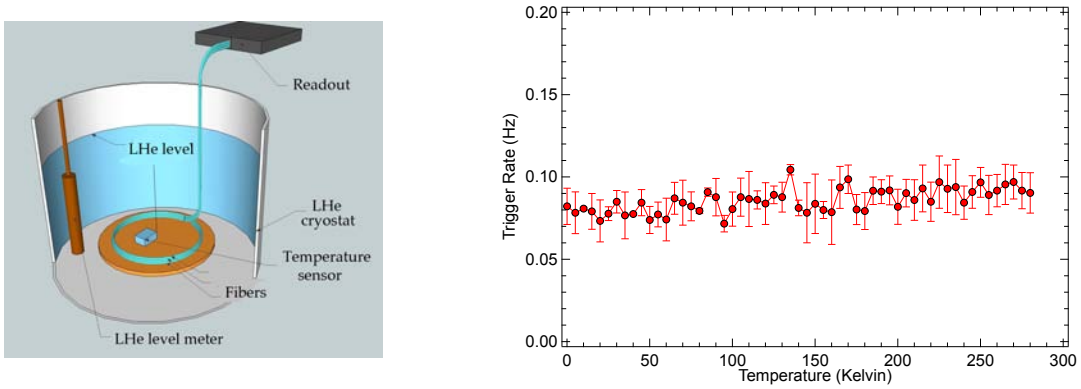

Figure 2.17: *Left: Equipment used to measure the performance of scintillating fibers at cryogenic temperatures. Right: Trigger rate of a scintillating fiber from cosmic rays as a function of temperature (see text).*

We are also investigating (in collaboration with the Albert Einstein Center in Bern) the possibility to use photographic emulsions of the OPERA type to reconstruct more accurately the interference pattern in the gravitation experiment. We would measure the annihilation points of $\bar{H}$- atoms on the vacuum exit window behind the Moiré deflectometer, using two or more annihilation pions. The emulsion stack would be placed immediately behind a very thin window separating the UHV vacuum from normal vacuum. The time-of-flight and the approximate track positions would be determined

by a silicon or scintillating fiber detector located outside the vacuum enclosure and stored for offline analysis. The emulsions would then be removed periodically and processed in Bern. Figure 2.18 shows the expected vertical resolution on the annihilation point due to multiple scattering as a function of window thickness (neglecting distortions and alignment errors). The Monte Carlo simulation indicates that r.m.s position resolutions of 3 μm could be achieved on the annihilation vertex, much better than the required 10 μm, thus allowing a more accurate measurement of $\bar{g}$.

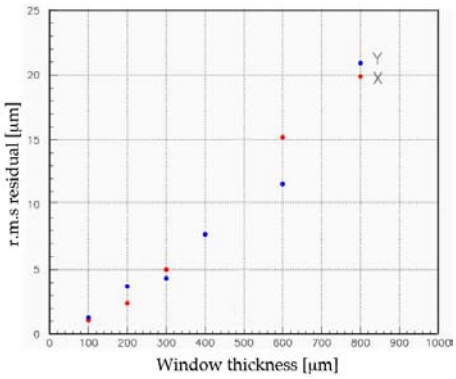

Figure 2.18: *R.m.s. position resolution on annihilation tracks as a function of thickness for a titanium vacuum window in which the $\bar{H}$-atoms annihilate.*

However, technical issues such as the performance of emulsions in vacuum (in particular dehydration) need to be investigated first. Also the background rate in the AD hall due to muons from the antiproton production target and from annihilation pions in the AEgIS apparatus need to be measured to assess the frequency at which emulsions would need to be changed. In 2012 we will commission the FACT detector and perform several test with photographic emulsions to plan for the first measurement of $\bar{g}$ after the 2013 maintenance of the CERN accelerators.

References

[1] Proposal: http://doc.cern.ch/archive/electronic/cern/preprints/spsc/public/spsc-2007-017.pdf
[2] E. Fischbach and C.L. Talmadge,"The Search for Non-Newtonian Gravity", Springer (1999)
[3] M. M. Nieto and T. Goldman, Phys. Rep. **205** (1991) 221
[4] M. Charlton, Phys. Lett. **A 143** (1990) 143
[5] E. Vliegen F. and Merkt, Phys. Rev. Lett **97** (2006) 033002
[6] Kuraray, http://www.kuraray.co.jp/en/
[7] Hamamatsu Photonics, http://www.hamamatsu.com/

3 Towards a dark matter experiment

Y. Allkofer, C. Amsler, W. Creus, A. Ferella, C. Regenfus, J. Rochet, and M. Walter.

We report on our research progress on liquid argon (LAr) which is part of the DARWIN design study [1] for a next generation dark matter facility using noble liquids. More details and references to earlier work can be found in a recent publication [2]. LAr has the potential to be used as a large and sensitive target to detect nuclear recoils from Weak Interacting Massive Particles (WIMP) interactions. WIMPs would produce nuclear recoils which can be detected and isolated in noble liquids through their characteristic excitation and ionisation patterns. The uncertainty in the signal calibration of nuclear recoils in LAr is large since only scarce information on the scintillation efficiency can be found in literature. In fact, the complex microscopic processes which lead to the scintillation and charge signals are not well understood at low energies.

The energy dependent light yield Y_{nr} of nuclear recoils is described by the relative scintillation efficiency $\mathcal{L}_{\text{eff}}$ which compares the light yield of electrons to that of nuclear recoils (by convention $\mathcal{L}_{\text{eff}}$ is measured at zero electric field). Its value is determined by the product of two quenching processes. Towards low energies, an increasing fraction of the recoil energy is lost to heat (nuclear quenching). The density of the excited or ionised states produced during the stopping process depends on their interaction (luminescence quenching). The light yield of electrons is not affected by nuclear effects and is linearly proportional to the energy deposit above some tens of keV. The relative scintillation efficiency is expressed as $\mathcal{L}_{\text{eff}} = E_{ee}/E_r$, where E_{ee} stands for the energy of an electron producing the same amount of light as a recoiling nucleus with energy E_r. In contrast to xenon, a separation of the scintillation signal in fast (τ_1 = 6 ns) and slow (τ_2 = 1.6 μs) components is possible in LAr. This effect is exploited to reduce background in LAr dark matter detectors.

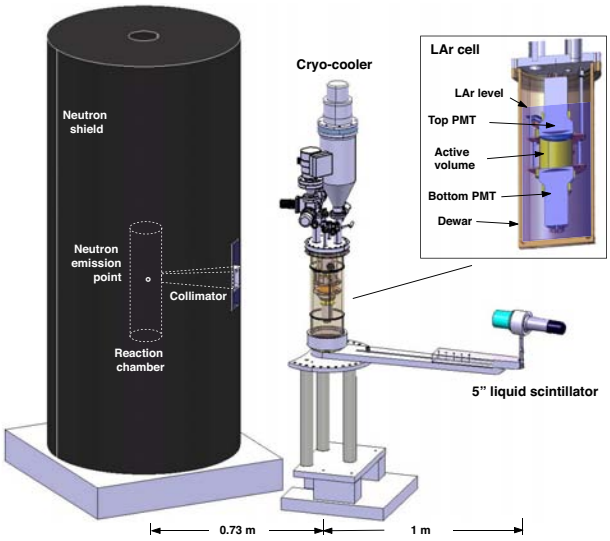

Figure 3.19: *$n - Ar$ scattering experiment with neutron generator, shield and zoom on the LAr cell.*

We present an overview of the experimental method to determine $\mathcal{L}_{\text{eff}}$ and show first results from data recorded under neutron, α and γ-irradiation in LAr at zero electric field. The experimental setup is shown in fig. 3.19. We induce nuclear recoils in the LAr cell by 2.45 MeV neutrons from a deuterium-fusion-generator (from NSD-Fusion, Germany). It delivers up to 2×10^6 isotropically emitted monoenergetic neutrons from the two-body reaction $\mathrm{dd} \rightarrow {}^3\mathrm{He} + \mathrm{n}$. The fusion rate in the deuterium plasma is controlled by an electrical DC field generated by an adjustable constant current

HV supply. The environment is shielded from neutron and X-ray radiation by a 1600 kg polyester cylinder with 2 mm Pb cladding. A polyethylene collimator with square cross section restricts the emission of neutrons in a solid angle of about 0.2% of 4π. Liquid scintillator counters (LSC) detect the scattered neutrons at various angles.

The cryogenic cell is shown in the inset. Two tetra-phenyl-butadiene (TPB) coated 3" PMTs (Hamamatsu R6091-MOD) with bialkali photo cathodes and Pt underlay (QE≈15%) are arranged face to face, forming a cylindrical sensitive volume of roughly 0.2ℓ. The cell walls are covered with a TPB coated reflector foil [3, 4] to shift the VUV scintillation light (128 nm) to $\sim$ 420 nm. A ^{210}Po α-source is installed in the center of the cell. A turbopump is used to evacuate the chamber to typically 10^{-6} mbar prior to filling with argon gas class 60. A membrane pump provides for recirculation via OXISORB cartridges which reduce the O_2 and H_2O contamination. The gas is condensed on top of the chamber by a (Sumitomo CH210) cryocooler. A LabView slow control regulates the cold head temperature and records temperatures, pressures and liquid levels.

The analogue signals from the two PMTs are each split into 2 inputs (for a larger dynamic range) and sampled with an oscilloscope with 5000 points at 1 GS/s. LAr signals are integrated numerically from the digitized currents of the PMTs, normalised to their mean single photon charges. Light yield calibrations were performed regularly with an external ^{241}Am source producing a prominent 60 keV photopeak.

In LAr VUV fluorescence from the so-called second continuum is the dominant mechanism for light emission. The light pulse shape is described by the sum of two exponentials with amplitudes describing the radiative decays of two fundamental excimer states (singlet and triplet, with lifetimes τ_1 and τ_2, respectively). Due to their long lifetime triplet states undergo collisions with neighbouring particles before decaying. Interactions with impurities can cause their (non-radiative) destruction, inducing losses in the slow scintillation light and a reduction in τ_2. In the following our component ratio (CR) – the relative strength of the fast component of the scintillation light – is corrected for this effect by extrapolation to pure LAr [2, 5].

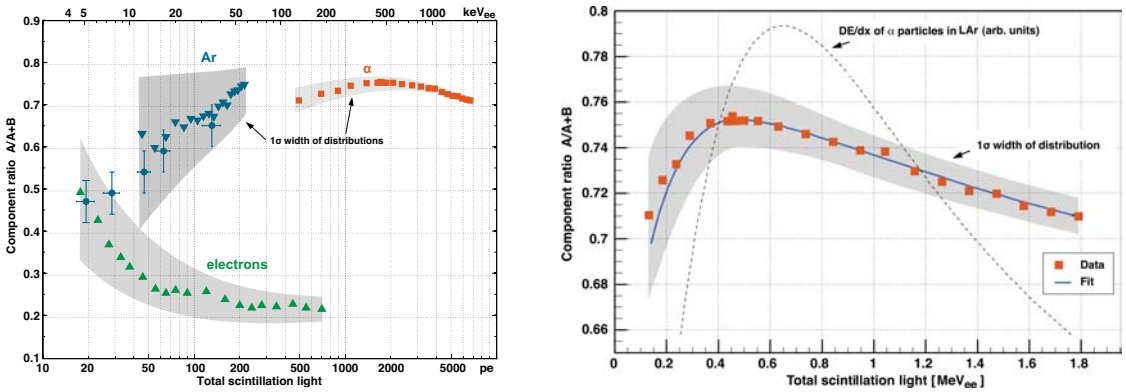

Figure 3.20: *Left: CR vs. light yield for Ar-, α-recoils and electrons. The grey zones indicate the 1σ spread. Right: CR for αs in LAr and fit vs. total scintillation light in MeV (electron equivalent).*

The CRs are determined for recoiling Ar nuclei (induced by neutrons), α-particles (from the ^{210}Po source) and electrons (induced by 511 keV γs from an external ^{22}Na source). A coincidence with an external detector was required for the photon data to tag the emission of two 511 keV γs. This data was also used to determine the time-of-flight calibration. Figure 3.20 (left) shows the CR distribution vs. total amount of scintillation light. The two prominent bands from electrons and nuclear recoils merge for energies below about 10 keV$_{ee}$. The values at low energies for argon recoils

are also shown (circles). There is a correlation between CR and the stopping power. Large ionisation densities lead to strong interaction between particles and produce a larger fraction of singlet states. For electrons CR is equal to $\sim$ 0.25 at the minimum ionisation densities, close to the statistical weights of 1 : 3 for the isolated production of singlet and triplet states (no interaction between them).

The relation between population of excimer states at various energy losses can be unfolded by taking into account the integral over the stopping range. We have determined the energy scale for α-particles by assuming a linear relation between CR and the energy transfer [2]. A value of $\mathcal{L}_{\rm eff}^{\alpha}$ = 0.74$\pm$0.04 was found for the mean relative scintillation efficiency for α-particles in LAr in the range 0.18 – 2.5 MeV (fig. 3.20, right). The light loss of $\simeq$ 25% is entirely due to luminescence quenching.

We now present the data taken with the neutron generator. A 5" liquid scintillator (LSC) was positioned at 30, 40, 50, 60 and 90°, at 1 m from the target, corresponding to 16, 28, 43, 60 and 120 keV recoil energies, respectively. The neutron flux (typically 2×10^5 n/s into 4π) was chosen so that accidental background induced by bremsstrahlung was kept at an acceptable level. About 1 n/min scattered off an argon nucleus in the active volume and was detected in the LSC. The direct line of sight between the exit of the collimator and the LSC was obstructed by a 20 cm thick sheet of polyethylene. Background rates were around 5/min, originating mainly from cosmic muons saturating the LSC, and accidental coincidences between diffusively scattered neutrons and bremsstrahlung. Events in the LAr cell were accepted whenever both PMTs showed signals above 0.2 photoelectrons (pe) in a 50 ns time coincidence. A trigger was generated by a LAr signal within a window of [-150, +50] ns around the arrival time of a neutron in the LSC.

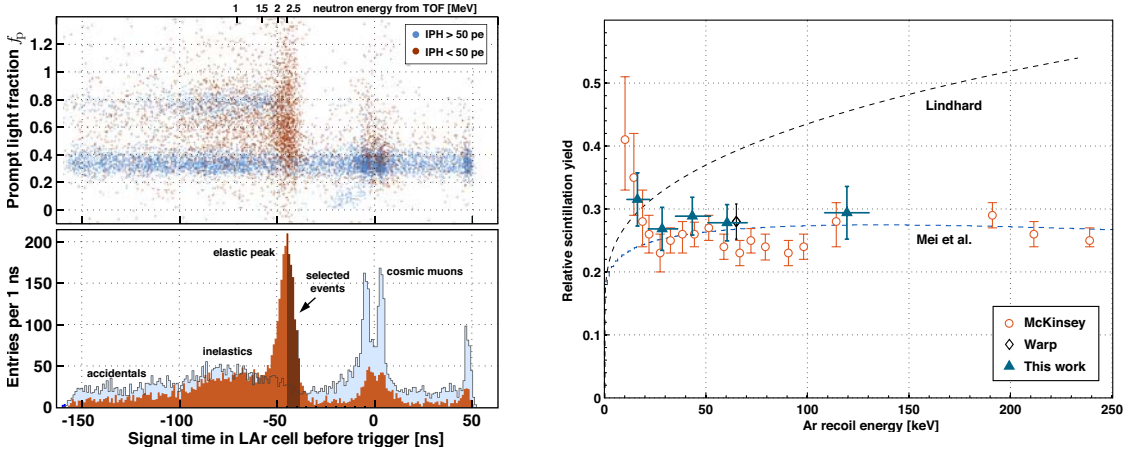

Figure 3.21: *Left: Prompt light fraction f_p vs. signal time in LAr and projection on the time axis for neutrons triggering the liquid scintillator counter. Right: $\mathcal{L}_{\rm eff}$ from this work compared to theory and previous data.*

Figure 3.21 (top) shows the prompt light fraction f_p vs. the time difference between the signals in the LAr cell and the LSC for the 30° data (19k events). Here f_p is the ratio of the scintillation light yield in the first 50 ns to the total light. The time projection is shown in fig. 3.21 (bottom). The distribution of signals ($<$ 50 pe) is dominated by elastically scattered neutrons around the nominal flight time at -45 ns (brown histogram). Also visible are inelastic scatters from neutrons and a small background from accidental coincidences of diffusely scattered neutrons with bremsstrahlung in the outer LAr volume. Requiring at most 50 pe removes many of these events and also cosmic muons (blue histogram). A 5 ns wide TOF cut then selects elastic scatters ($\sim$1'000 events, black area). Figure 3.21 (right) shows our measurements at the five angles, together with the data from refs. [6, 7]. Our measurements lead to the average $<\mathcal{L}_{\rm eff}>$ = 0.29 $\pm$ 0.03 for nuclear recoils above 20 keV (or 6 kev

electron equivalent). The data are consistent with a constant value for $\mathcal{L}_{\rm eff}$, in accord with a simple saturation law combined with the Lindhard model [8].

Summarizing, we confirm that scintillation light quenching in LAr by impurities is similar to that in gaseous argon [5]. As in the latter work we use measured lifetimes and component ratios to reconstruct purity independent results. We confirm values for CR monotonically increasing with energy transfer. A CR value of 0.25 close to the one expected from statistically populated singlet and triplet states is observed for electrons in the region of lowest ionisation densities. For nuclear recoils we find CR rising from 50% to 75% between 20 and 200 keV. For α-particles in the MeV range we determine a relative scintillation yield $\mathcal{L}_{\rm eff}^{\alpha}$ = 0.74$\pm$0.04. Within present errors our value of the relative scintillation yield $\mathcal{L}_{\rm eff}$ is constant for nuclear recoils at energies between 16 and 120 keV, with a mean value of 0.29$\pm$0.03. A refined analysis is in progress [9].

No conclusive results below 16 keV can be drawn from the present analysis. We are upgrading the cell with PMTs of larger quantum efficiency and are improving the cleaning system. An internal electric field will be added to extract the ionisation charge from the liquid and to determine field and energy dependences of both light and charge yields in LAr, at working points relevant to dark matter searches.

References

[1] L. Baudis, arXiv:1012.4764v1 [astro-ph.IM] (2010) and http://darwin.physik.uzh.ch/
[2] C. Regenfus *et al.*, arXiv:1203.0849v1 [astro-ph.IM] (2012)
[3] V. Boccone V *et al.*, J. of Instrumentation **4** (2009) P06001;
V. Boccone, PhD-thesis, Universität Zürich, 2010
[4] M. Walter, Diploma-Thesis, Universität Konstanz, 2011
[5] C. Amsler *et al.*, J. of Instrumentation **3** (2008) P02001
[6] R. Brunetti *et al.*, New Astr. Rev. **49** (2005) 265
[7] D. Gastler D *et al.*, arXiv:1004.0373v2 [physics.ins-det] (2011)
[8] D. Mei *et al.*, Astropart. Phys. **30** (2008) 12
[9] W. Creus, PhD-Thesis, Universität Zürich (in preparation)

4 Study of Coulomb-bound πK-pairs

C. Amsler, A. Benelli, and J. Rochet.

In collaboration with:
CERN, Czech Technical University, Institute of Physics and Nuclear Physics Institute ASCR (Czech Republic), Laboratori Nazionali di Frascati, Messina University, Trieste University, KEK, Kyoto Sangyo University, Tokyo Metropolitan University, IFIN-HH (Bucharest), JINR (Dubna), Skobeltsin Institute for Nuclear Physics (Moscow), IHEP (Protvino), Santiago de Compostela University, Bern University.

(DIRAC Collaboration)

We have observed for the first time in 2007 electromagnetically bound $\pi^{\mp}K^{\pm}$-pairs ($\pi^{\mp}K^{\pm}$-atoms) [1, 2]. The π^+K^--atom is unstable and decays through the strong force into $\pi^0\bar{K}^0$ (while π^-K^+-atoms decay into π^0K^0). The mean life τ, which we intend to measure, is related to the S-wave πK-scattering lengths a_1 and a_3 in the isospin 1/2 and 3/2 states, respectively. The πK-scattering length is of interest to test chiral perturbation theories extended to the s-quark. From the 2007 data sample we reported the observation of 173 $\pm$ 54 πK-pairs [1, 2]. This result led to a lower limit for the mean life of πK-atoms of 0.8 fs in the $1s$-state, which could be translated into an upper limit of the difference in scattering lengths $|a_1 - a_3| < 0.58\ m_\pi^{-1}$.

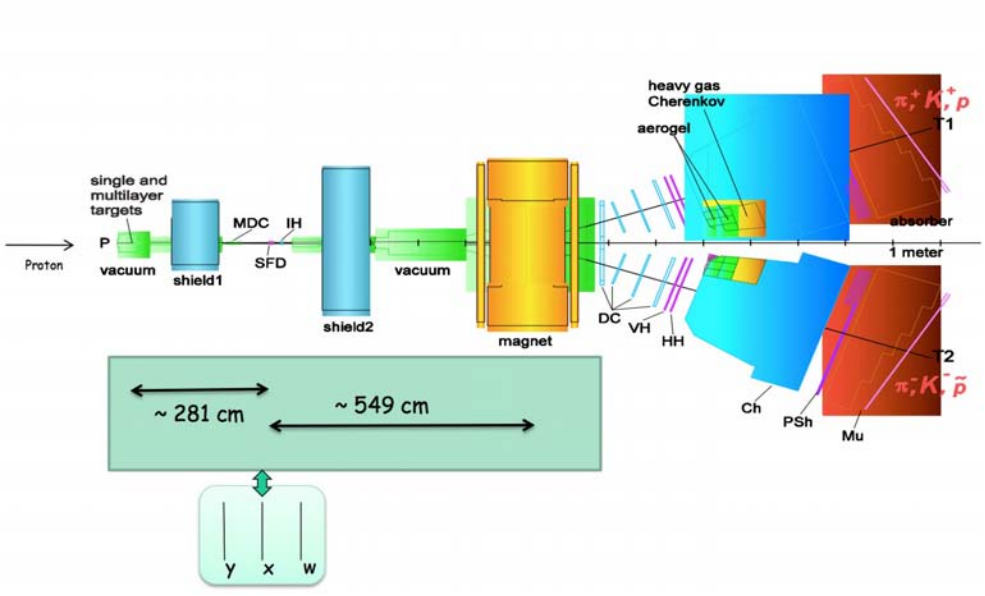

Figure 4.22: *Sketch of the updated DIRAC-II spectrometer, showing the locations of the Čerenkov counters to identify electrons, pions and kaons. MDC = microdrift chambers, SFD = scintillator fiber detector, IH = ionization hodoscope, DC = drift chambers, VH, HH = vertical and horizontal scintillation hodoscopes, CH = N_2-Čerenkov counter, PSh = preshower, Mu = muon counters.*

The DIRAC experiment was initially designed to study $\pi^+\pi^-$-atoms. Final results for $\pi^+\pi^-$ have been published recently [3]. From a sample of 21'227 $\pi^+\pi^-$ atomic pairs the difference in the isospin 0 and 2 scattering lengths could be measured with a 4% accuracy, $|a_0 - a_2|$ = 0.2533 $\pm$ 0.0109 m_π^{-1}. The corresponding mean life is 3.15 $\pm$ 0.28 fs. An overview of the DIRAC experiment can be found in ref. [4].

A sketch of the DIRAC spectrometer to collect πK (and also more $\pi\pi$) data is shown in fig. 4.22. Details can be found in previous annual reports and also in ref. [5]. The 24 GeV/c proton beam from the CERN-PS passes through a thin (100 μm) Ni-target. The secondary particles traverse a scintillation fiber detector (SFD) and a ionization hodoscope (IH) with which the opening angle between pairs of secondaries can be measured. The pions and kaons are analyzed in a double-arm magnetic spectrometer measuring the momentum vectors of two oppositely charged hadrons. Positive particles are deflected into the left arm, negative ones into the right arm. The spectrometer is slightly tilted upwards with respect to the proton beam. Electrons and positrons are vetoed by the N_2-Čerenkov detectors and muons by their signals in scintillation counters behind steel absorbers. Kaons are separated from pions and protons by heavy gas (C_4F_{10}) Čerenkov counters (which fire on pions) and by aerogel Čerenkov counters (which fire on both pions and kaons, but not not on the more numerous protons). Our group has developed and built the 37ℓ aerogel Čerenkov counter [6] and the gas system for the C_4F_{10} counters [7]. The signal from πK-atoms is observed for πK-pairs with a very small relative momentum (typically $|Q_L| < 3$ MeV/c is the c.m.s system).

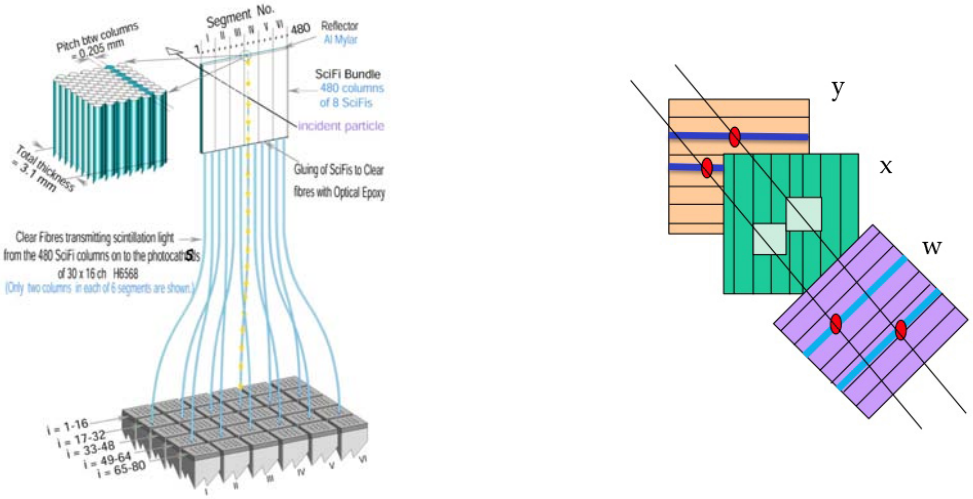

Figure 4.23: *Left: sketch of the SFD (x- and y-planes). Right: Measurement of the SFD performance with 2 out of 3 planes.*

In 2007 we used only the detectors downstream of the magnet, but the scintillation fiber detector (SFD) was available for the 2008 – 2010 run to determine the interaction point in the production target with much better precision. The SFD (fig. 4.23, left) consists of 3 planes of 205 μm scintillating fibers. Two planes (x- and y-planes) are made of 8 layers each with 480 fibers while the third (w-plane) contains 3 layers of 320 fibers. The fibers are read out in columns of 8, respectively 3 fibers by 30 $\times$ 16 Hamamatsu H6568 photomultipliers. The area covered by each plane is about 10 $\times$ 10 cm^2 and contributes only 1% radiation length. The timing resolution is 460 ps. Tracks are measured with good resolution (σ = 60 μm) and high efficiency (98%). This leads to a substantial improvement in the resolution on the transverse momentum Q_T (from 3 MeV/c to 1 MeV/c) and also reduces the background.

During 2010 we tuned the Monte Carlo simulation of the SFD and compared with data. A substantial improvement has been achieved (for more details see ref. [8]). Noise, cross-talk between fibers, efficiency and background tracks have been inserted into the simulation. The simulated data were then submitted to the same analysis code as the experimental data. To study the performance of the SFD we used in turn two planes (e.g. y and w). The reconstructed tracks were then extrapolated

to the third plane (e.g. x, see fig. 4.23, right) and the measured hits compared with the predicted ones.

The excellent agreement between data and Monte Carlo is illustrated in fig. 4.24. The left plot shows the probability to find one hit within $\pm$ 1 mm around the extrapolated tracks. The right plot shows the probability to find both hits in the third plane for two tracks in the first two planes. The loss in the center is due to a hardware suppression algorithm of fiber cross-talks. The ionization hodoscope (IH) can be used to reduce background and select true double hits. From these plots one obtains track resolutions for the 2008-9-10 data of σ = 220 μm for single tracks and 550 μm for double tracks.

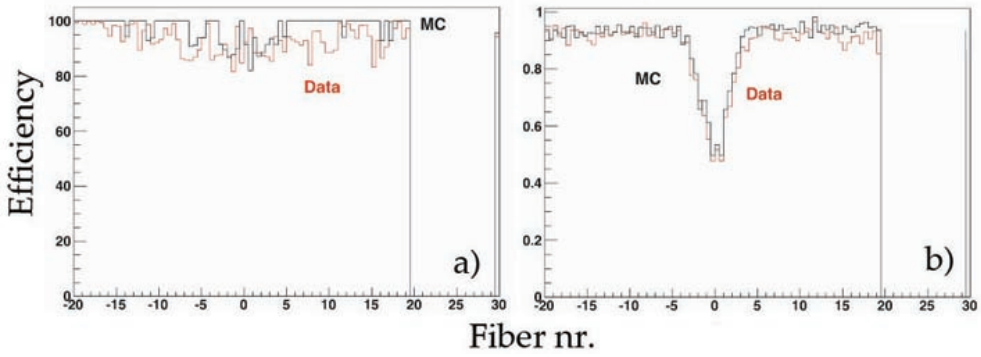

Figure 4.24: *a) Probability to find one hit in the x-plane around the extrapolated track; b) probability to find both hits for two tracks. Real data are shown in red, simulated data in black.*

Thus the SFD performed as expected from simulations and we could proceed with the analysis of the data using the three planes. We obtain a Q_x and Q_y resolution better than 0.5 MeV/c and reconstruct the momentum transfer Q between the kaon and the pion with a resolution of 1 MeV/c. As a calibration tool and momentum resolution measurement we reconstruct Λ decays into $\pi^- p$. The mass distribution shown in fig. 4.25 confirms the correct energy scale, the value for the Λ mass 1115.7 $\pm$ 0.5 MeV being fully compatible with the PDG value (1115.683 $\pm$ 0.006 MeV).

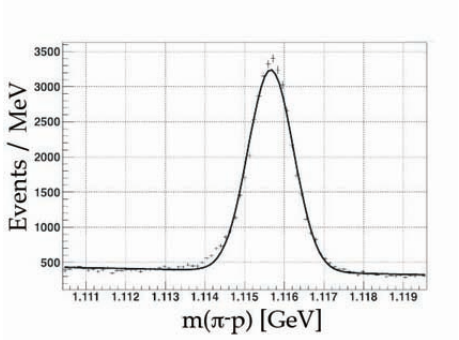

Figure 4.25: *Invariant $\pi^- p$ mass distribution showing the Λ signal.*

Clean πK events are selected by the SFD and IH detectors to resolve the ambiguity of single and double tracks in the upstream part of the apparatus (fig. 4.22). Particle identification is performed using the heavy gas and aerogel Čerenkov detectors. The precise time difference between the two tracks from the atomic candidates pairs is achieved using the VH. Events with muons or electrons are eliminated using the nitrogen Črenkov and muon detectors. We finally select events with relative transverse and longitudinal momenta between the two mesons of $Q_T < 4$ MeV/c and $|Q_l| < 20$

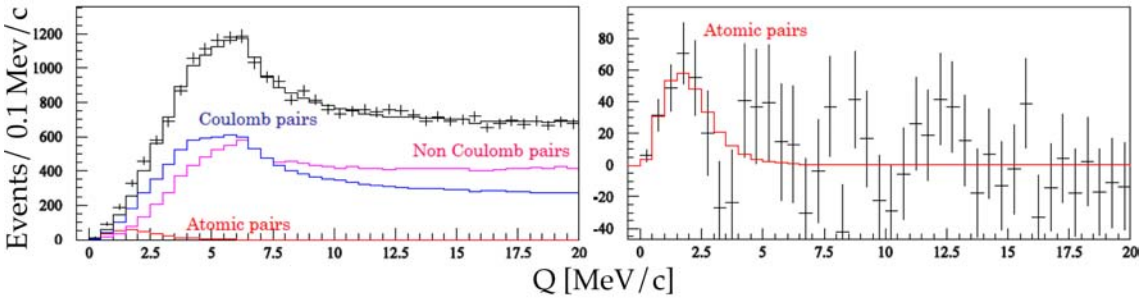

Figure 4.26: $\pi^- K^+ + \pi^+ K^-$ *events as a function of relative momentum* Q*. The enhancement at low* Q *in the bottom plot is due to* πK *atomic pairs.*

MeV/c, repectively. Figure 4.26 (left) shows the preliminary distribution of $\pi^- K^+ + \pi^+ K^-$ events as a function of relative momentum Q (points with error bars).

The fit results are shown in red (atomic pairs), blue (Coulomb pairs), magenta (non-Coulomb pairs). The sum of Coulomb and non Coulomb pairs is displayed in black. The contribution from atomic pairs is shown in red in fig. 4.26 (right). We find 277 $\pm$ 52 atomic pairs to be compared with 173 $\pm$ 54 from the 2007 run. However, in 2007 our goal was the first observation of πK-atoms and hence a target was chosen (Pt) for which the production cross section was high. The breakup probability for πK-atoms as a function of mean life (53% for 3.7 fs) is flattening off above $\sim$ 4 fs. Therefore we could only give a lower limit for the mean life of πK-atoms. Instead we used in 2008-9-10 a Ni-target which produces fewer atoms but for which the dependence between breakup probability and mean life is described by a steeper function, thus allowing a more accurate measurement of the mean life.

The final analysis of the 2008 – 2010 data is in progress. Due to a slow degradation of the light (n = 1.008) aerogel with time (probably due to humidity), we could only use the $n = 1.015$ aerogel and had therefore to restrict the maximum kaon momentum to 5.5 GeV/c, thus unfortunately reducing statistics. Also, a recalibration of the preshower detector (Psh) is required to suppress background from electron-positron pairs which is significant in the new data. Data taking for the DIRAC experiment will be completed in autumn 2012.

References

[1] B. Adeva *et al.* (DIRAC Collaboration), Phys. Lett. **B 674** (2009) 11
[2] Y. Allkofer, PhD Thesis, University of Zurich (2008)
[3] B. Adeva *et al.* (DIRAC Collaboration), Phys. Lett. **B 704** (2011) 24
[4] J. Schacher, CERN courier, March 2012, p. 24
[5] B. Adeva *et al.* (DIRAC Collaboration), Nucl. Instrum. Methods in Phys. Res. **A 515** (2003) 467
[6] Y. Allkofer *et al.*, Nucl. Instr. Meth. in Phys. Res. **A 582** (2007) 497;
Y. Allkofer *et al.*, Nucl. Instr. Meth. in Phys. Res. **A 595** (2008) 84;
C. Amsler, Proc. of Science PoS EPS-HEP (2009) 078
[7] S. Horikawa *et al.*, Nucl. Instr. Meth. in Phys. Res. **A 595** (2008) 212
[8] A. Benelli, http://dirac.web.cern.ch/DIRAC/talk/talk1101.pdf

5 Publications

Articles[3]

1. **Towards the production of an ultra cold antihydrogen beam with the AEGIS apparatus**
   J. W. Storey
   Hyperfine Interact, DOI 10.1007/s10751-011-0401-x

2. **The AEGIS experiment at CERN, measuring the free fall of antihydrogen**
   A. Kellerbauer et al. (AEGIS Collaboration)
   Hyperfine Interact, DOI 10.1007/s10751-012-0583-x

3. **Off-axial plasma displacement suitable for antihydrogen production in AEgIS experiment**
   C. Canali et al. (AEGIS Collaboration)
   Eur. Phys. J. **D 65** (2011) 499

4. **Determination of $\pi\pi$ scattering lengths from measurement of the $\pi\pi$ atom lifetime**
   B. Adeva et al. (DIRAC Collaboration)
   Phys. Lett. **B 704** (2011) 24

5. **A new CMS pixel detector for the LHC luminosity upgrade**
   C. Favaro
   Nucl. Instr. and Meth. **A 658** (2011) 41

6. **Performance of the CMS pixel detector from the first LHC collisions**
   S. de Visscher
   Nuclear Physics B - Proc. Suppl. **215** (2011) 101

7. **Measurement of exclusive b-hadron production at 7 TeV with the CMS experiment**
   E. Aguiló
   PoS (BEAUTY 2011) 003

8. **The Alignment of the CMS Silicon Tracker**
   E. Aguiló
   Nuclear Physics B - Proc. Suppl. **215** (2011) 104

9. **CMS Detector Performance**
   H. Snoek
   PoS (BEAUTY 2011) 048

10. **Measurement of tau identification efficiency at CMS**
    M. Verzetti
    PoS (EPS-HEP2011) 417

11. **Performance of track and vertex reconstruction and b-tagging studies with CMS in pp collisions at $\sqrt{s}$ = 7 TeV**
    A. Schmidt
    PoS (Kruger 2010) 032

12. Search for Stopped Gluinos in pp collisions at $\sqrt{s} = 7$ TeV
    CMS Collaboration
    Phys. Rev. Lett. **106** (2011) 011801

[3] Articles with substantial contributions from the Zurich group are in boldface.

13. Measurement of the Isolated Prompt Photon Production Cross Section in pp Collisions at $\sqrt{s} =$ 7 TeV
CMS Collaboration
Phys. Rev. Lett. **106** (2011) 082001

14. **Measurement of the B^+ Production Cross Section in pp Collisions at $\sqrt{s} = 7$ TeV**
CMS Collaboration
Phys. Rev. Lett. **106** (2011) 112001

15. Dijet Azimuthal Decorrelations in pp Collisions at $\sqrt{s} = 7$ TeV
CMS Collaboration
Phys. Rev. Lett. **106** (2011) 122003

16. Search for Pair Production of First-Generation Scalar Leptoquarks in pp Collisions at $\sqrt{s} = 7$ TeV
CMS Collaboration
Phys. Rev. Lett. **106** (2011) 201802

17. Search for Pair Production of Second-Generation Scalar Leptoquarks in pp Collisions at $\sqrt{s} =$ 7 TeV
CMS Collaboration
Phys. Rev. Lett. **106** (2011) 201803

18. Measurement of Dijet Angular Distributions and Search for Quark Compositeness in pp Collisions at $\sqrt{s} = 7$ TeV
CMS Collaboration
Phys. Rev. Lett. **106** (2011) 201804

19. Search for Supersymmetry in pp Collisions at $\sqrt{s} = 7$ TeV in Events with Two Photons and Missing Transverse Energy
CMS Collaboration
Phys. Rev. Lett. **106** (2011) 211802

20. Study of Z boson production in PbPb collisions at $\sqrt{s_{NN}}$= 2.76 TeV
CMS Collaboration
Phys. Rev. Lett. **106** (2011) 212301

21. **Search for Neutral MSSM Higgs Bosons Decaying to Tau Pairs in pp Collisions at $\sqrt{s}$ =7 TeV**
CMS Collaboration
Phys. Rev. Lett. **106** (2011) 231801

22. **Measurement of the B^0 Production Cross Section in pp Collisions at $\sqrt{s}$ = 7 TeV**
CMS Collaboration
Phys. Rev. Lett. **106** (2011) 252001

23. Measurement of the Polarization of W Bosons with Large Transverse Momenta in W+Jets Events at the LHC
CMS Collaboration
Phys. Rev. Lett. **107** (2011) 021802

24. Indication of suppression of excited states in PbPb collisions at $\sqrt{s}$ = 2.76 TeV
CMS Collaboration
Phys. Rev. Lett. **107** (2011) 052302

25. Measurement of the t-channel single top quark production cross section in pp collisions at $\sqrt{s}$ = 7 TeV
CMS Collaboration
Phys. Rev. Lett. **107** (2011) 091802

26. Search for Three-Jet Resonances in pp Collisions at $\sqrt{s}$ = 7 TeV
CMS Collaboration
Phys. Rev. Lett. **107** (2011) 101801

27. Measurement of the Inclusive Jet Cross Section in pp Collisions at $\sqrt{s}$ = 7 TeV
CMS Collaboration
Phys. Rev. Lett. **107** (2011) 132001

28. **Search for $B_s^0 \to \mu^+\mu^-$ and $B^0 \to \mu^+\mu^-$ decays in pp collisions at $\sqrt{s}$ = 7 TeV**
CMS Collaboration
Phys. Rev. Lett. **107** (2011) 191802

29. Search for New Physics with a Mono-Jet and Missing Transverse Energy in pp Collisions at $\sqrt{s}$ = 7 TeV
CMS Collaboration
Phys. Rev. Lett. **107** (2011) 201804

30. Search for Supersymmetry at the LHC in Events with Jets and Missing Transverse Energy
CMS Collaboration
Phys. Rev. Lett. **107** (2011) 221804

31. Search for a Vectorlike Quark with Charge 2/3 in $t + Z$ Events from pp Collisions at $\sqrt{s}$ = 7 TeV
CMS Collaboration
Phys. Rev. Lett. **107** (2011) 271802

32. Search for signatures of extra dimensions in the diphoton mass spectrum at the Large Hadron Collider
CMS Collaboration
Phys. Rev. Lett. **108** (2012) 111801

33. Measurement of the Inclusive Upsilon production cross section in pp collisions at $\sqrt{s}$ = 7 TeV
CMS Collaboration
Phys. Rev. **D 83** (2011) 112004

34. Observation and studies of jet quenching in PbPb collisions at nucleon-nucleon center-of-mass energy = 2.76 TeV
CMS Collaboration
Phys. Rev. **C 84** (2011) 024906

35. **Measurement of the B_s^0 Production Cross Section with $B_s^0 \to J/\psi\phi$ Decays in pp Collisions at $\sqrt{s}$ = 7 TeV**
CMS Collaboration
Phys. Rev. **D 84** (2011) 052008

36. Measurement of the Differential Cross Section for Isolated Prompt Photon Production in pp Collisions at 7 TeV
CMS Collaboration
Phys. Rev. **D 84** (2011) 052011

37. Measurement of the $t\bar{t}$ Production Cross Section in pp Collisions at 7 TeV in Lepton + Jets Events Using b-quark Jet Identification
CMS Collaboration
Phys. Rev. **D 84** (2011) 092004

38. Measurement of the weak mixing angle with the Drell-Yan process in proton-proton collisions at the LHC
CMS Collaboration
Phys. Rev. **D 84** (2011) 112002

39. Inclusive search for squarks and gluinos in pp collisions at $\sqrt{s}$ = 7 TeV
CMS Collaboration
Phys. Rev. **D 85** (2012) 012004

40. Measurement of the Rapidity and Transverse Momentum Distributions of Z Bosons in pp Collisions at $\sqrt{s}$ = 7 TeV
CMS Collaboration
Phys. Rev. **D 85** (2012) 032002

41. First Measurement of the Cross Section for Top-Quark Pair Production in Proton-Proton Collisions at $\sqrt{s} = 7$ TeV
CMS Collaboration
Phys. Lett. **B 695** (2011) 424

42. Search for Microscopic Black Hole Signatures at the Large Hadron Collider
CMS Collaboration
Phys. Lett. **B 697** (2011) 434

43. Search for a heavy gauge boson W' in the final state with an electron and large missing transverse energy in pp collisions at $\sqrt{s} = 7$ TeV
CMS Collaboration
Phys. Lett. **B 698** (2011) 21

44. **Search for Supersymmetry in pp Collisions at 7 TeV in Events with Jets and Missing Transverse Energy**
CMS Collaboration
Phys. Lett. **B 698** (2011) 196

45. Measurement of W^+W^- Production and Search for the Higgs Boson in pp Collisions at $\sqrt{s} =$ 7 TeV
CMS Collaboration
Phys. Lett. **B 699** (2011) 25

46. First Measurement of Hadronic Event Shapes in pp Collisions at $\sqrt{s} = 7$ TeV
CMS Collaboration
Phys. Lett. **B 699** (2011) 48

47. Measurement of the Tau pairs production cross section in proton-proton collisions at $\sqrt{s}$ =7 TeV
CMS Collaboration
Phys. Lett. **B 700** (2011) 187

48. Search for a W' boson decaying to a muon and a neutrino in pp collisions at $\sqrt{s} = 7$ TeV
CMS Collaboration
Phys. Lett. **B 701** (2011) 160

49. Search for a Heavy Bottom-like Quark in pp Collisions at $\sqrt{s} = 7$ TeV
CMS Collaboration
Phys. Lett. **B 701** (2011) 204

50. Measurement of Wγ and Zγ production in pp collisions at $\sqrt{s}$ = 7 TeV
CMS Collaboration
Phys. Lett. **B 701** (2011) 535

51. Measurement of the Ratio of the 3-jet to 2-jet Cross Sections in pp Collisions at $\sqrt{s}$ = 7 TeV
CMS Collaboration
Phys. Lett. **B 702** (2011) 336

52. Search for First Generation Scalar Leptoquarks in the $e?jj$ Channel in pp Collisions at $\sqrt{s}$ = 7 TeV
CMS Collaboration
Phys. Lett. **B 703** (2011) 246

53. A search for excited leptons in pp Collisions at $\sqrt{s}$ = 7 TeV
CMS Collaboration
Phys. Lett. **B 704** (2011) 143

54. Search for Physics Beyond the Standard Model Using Multilepton Signatures in pp Collisions at $\sqrt{s}$ =7 TeV
CMS Collaboration
Phys. Lett. **B 704** (2011) 411

55. Measurement of the charge asymmetry in top-quark pair production in proton-proton collisions at $\sqrt{s}$ = 7 TeV
CMS Collaboration
Phys. Lett. **B 709** (2012) 28

56. Combined results of searches for the standard model Higgs boson in pp collisions at $\sqrt{s} =$ 7 TeV
CMS Collaboration
Phys. Lett. **B 710** (2012) 26

57. Search for the standard model Higgs boson decaying to W^+W^- in the fully leptonic final state in pp collisions at $\sqrt{s} = 7$ TeV
CMS Collaboration
Phys. Lett. **B 710** (2012) 91

58. Search for the standard model Higgs boson decaying to bottom quarks in pp collisions at $\sqrt{s} =$ 7 TeV

CMS Collaboration
Phys. Lett. **B 710** (2012) 284

59. Measurement of isolated photon production in pp and PbPb collisions at $\sqrt{s_{NN}} = 2.76$ TeV
CMS Collaboration
Phys. Lett. **B 710** (2012) 256

60. Charged particle multiplicities in pp interactions at $\sqrt{s}$ = 0.9, 2.36, and 7 TeV
CMS Collaboration
J. High Energy Physics **01** (2011) 079

61. Measurements of Inclusive W and Z Cross Sections in pp Collisions at $\sqrt{s} = 7$ TeV
CMS Collaboration
J. High Energy Physics **01** (2011) 080

62. Search for Heavy Stable Charged Particles in pp collisions at $\sqrt{s}$ = 7 TeV
CMS Collaboration
J. High Energy Phys. **03** (2011) 024

63. **Inclusive b-hadron production cross section with muons in pp collisions at $\sqrt{s}$ = 7 TeV**
CMS Collaboration
J. High Energy Phys. **03** (2011) 090

64. **Measurement of $B\bar{B}$ angular correlations based on secondary vertex reconstruction at $\sqrt{s}$ = 7 TeV**
CMS Collaboration
J. High Energy Phys. **03** (2011) 136

65. Measurement of the lepton charge asymmetry in inclusive W production in pp collisions at $\sqrt{s} = 7$ TeV
CMS Collaboration
J. High Energy Phys. **04** (2011) 050

66. Measurement of Bose-Einstein Correlations in pp Collisions at $\sqrt{s} = 0.9$ and 7 TeV
CMS Collaboration
J. High Energy Phys. **05** (2011) 029

67. Strange Particle Production in pp Collisions at $\sqrt{s} = 0.9$ and 7 TeV
CMS Collaboration
J. High Energy Phys. **05** (2011) 064

68. Search for Large Extra Dimensions in the Diphoton Final State at the Large Hadron Collider
CMS Collaboration
J. High Energy Phys. **05** (2011) 085

69. Search for Resonances in the Dilepton Mass Distribution in pp Collisions at $\sqrt{s} = 7$ TeV
CMS Collaboration
J. High Energy Phys. **05** (2011) 093

70. Search for Physics Beyond the Standard Model in Opposite-sign Dilepton Events in pp Collisions at $\sqrt{s}$ = 7 TeV
CMS Collaboration
J. High Energy Phys. **06** (2011) 026

71. Search for new physics with same-sign isolated dilepton events with jets and missing transverse energy at the LHC
CMS Collaboration
J. High Energy Phys. **06** (2011) 077

72. Search for supersymmetry in events with a lepton, a photon, and large missing transverse energy in pp collisions at $\sqrt{s}$ = 7 TeV
CMS Collaboration
J. High Energy Phys. **06** (2011) 093

73. Measurement of the $t\bar{t}$ production cross section and the top quark mass in the dilepton channel in pp collisions at $\sqrt{s}$ =7 TeV
CMS Collaboration
J. High Energy Phys. **07** (2011) 049

74. Long-range and short-range dihadron angular correlations in central PbPb collisions at $\sqrt{s_{NN}}$ = 2.76 TeV
CMS Collaboration
J. High Energy Phys. **07** (2011) 076

75. Search for Light Resonances Decaying into Pairs of Muons as a Signal of New Physics
CMS Collaboration
J. High Energy Phys. **07** (2011) 098

76. Search for Supersymmetry in Events with b Jets and Missing Transverse Momentum at the LHC
CMS Collaboration
J. High Energy Phys. **07** (2011) 113

77. Search for Same-Sign Top-Quark Pair Production at $\sqrt{s}$ = 7 TeV and Limits on Flavour Changing Neutral Currets in the Top Sector
CMS Collaboration
J. High. Energy Phys. **08** (2011) 005

78. Charged particle transverse momentum spectra in pp collisions at $\sqrt{s}$ = 0.9 and 7 TeV
CMS Collaboration
J. High Energy Phys. **08** (2011) 086

79. Measurement of the Inclusive Z Cross Section via Decays to Tau Pairs in pp Collisions at $\sqrt{s}$ = 7 TeV
CMS Collaboration
J. High Energy Phys. **08** (2011) 117

80. Dependence on pseudorapidity and on centrality of charged hadron production in PbPb collisions at $\sqrt{s_{NN}}$ = 2.76 TeV
CMS Collaboration
J. High Energy Phys. **08** (2011) 141

81. Search for New Physics with Jets and Missing Transverse Momentum in pp collisions at $\sqrt{s}$ = 7 TeV
CMS Collaboration
J. High Energy Phys. **08** (2011) 155

82. Search for supersymmetry in pp collisions at $\sqrt{s}$ = 7 TeV in events with single lepton, jets, and missing transverse momentum CMS Collaboration
J. High Energy Phys. **08** (2011) 156

83. Measurement of the Underlying Event Activity at the LHC with $\sqrt{s}$ = 7 TeV and Comparison with $\sqrt{s}$ = 0.9 TeV
CMS Collaboration
J. High Energy Phys. **09** (2011) 109

84. Measurement of the Drell-Yan Cross Section in pp Collisions at $\sqrt{s}$ = 7 TeV
CMS Collaboration
J. High Energy Phys. **10** (2011) 007

85. Measurement of the Inclusive W and Z Production Cross Sections in pp Collisions at $\sqrt{s}$ = 7 TeV with the CMS experiment
CMS Collaboration
J. High Energy Phys. **10** (2011) 132

86. Measurement of energy flow at large pseudorapidities in pp collisions at $\sqrt{s}$ = 0.9 and 7 TeV
CMS Collaboration
J. High Energy Phys. **11** (2011) 148

87. Jet Production Rates in Association with W and Z Bosons in pp Collisions at $\sqrt{s}$ = 7 TeV
CMS Collaboration
J. High Energy Phys. **01** (2012) 010

88. Exclusive $\gamma\gamma \to \mu^+\mu^-$ production in proton-proton collisions at $\sqrt{s} = 7$ TeV
CMS Collaboration
J. High Energy Phys. **01** (2012) 052

89. Measurement of the Production Cross Section for Pairs of Isolated Photons in pp collisions at$\sqrt{s}$= 7 TeV
CMS Collaboration
J. High Energy Phys. **01** (2012) 133

90. J/ψ **and** $\psi(2S)$ **production in** pp **collisions at** $\sqrt{s}$ **= 7 TeV**
CMS Collaboration
J. High Energy Phys. **02** (2012) 011

91. **Prompt and non-prompt J/psi production in** pp **collisions at** $\sqrt{s} = 7$ **TeV**
CMS Collaboration
Eur. Phys. J. **C 71** (2011) 1575

92. Measurement of the $t\bar{t}$ Production Cross Section in pp Collisions at $\sqrt{s}$=7 TeV using the Kinematic Properties of Events with Leptons and Jets
CMS Collaboration
Eur. Phys. J. **C 71** (2011) 1721

93. Forward Energy Flow, Central Charged-Particle Multiplicities, and Pseudorapidity Gaps in W and Z Boson Events from pp Collisions at $\sqrt{s}$= 7 TeV
CMS Collaboration
Eur. Phys. J. **C 72** (2012) 1839

94. Missing transverse energy performance of the CMS detector
CMS Collaboration
Journal of Instrumentation **6** (2011) P09001

95. Determination of Jet Energy Calibration and Transverse Momentum Resolution in CMS
CMS Collaboration
Journal of Instrumentation **6** (2011) P11002

96. Performance of τ-lepton reconstruction and identification in CMS
CMS Collaboration
Journal of Instrumentation **7** (2012) P01001

Articles in press

1. **Heavy flavor physics with the CMS experiment**
V. Chiochia
Proceedings of the 2011 Hadron Collider Physics symposium, Paris (2011)
Pre-print: arXiv.org/abs/1201.6677

2. **Search for WIMPs in liquid argon**
C. Amsler
Proceedings of the WIN11 Conference, Cape Town (2011)
Pre-print: arXiv.org/abs/1105.4524

3. **Study of nuclear recoils in liquid argon with monoenergetic neutrons**
C. Regenfus, Y. Allkofer, C. Amsler, W. Creus, A. Ferella, J. Rochet, M. Walter
To appear in Journal of Physics: Conference Series (JCPS)
Pre-print: arXiv:1203.0849v1 [astro-ph.IM]

4. **Scalar mesons below 2 GeV**
C. Amsler, S. Eidelman, T. Gutsche, C. Hanhart, S. Spanier and N.A. Törnqvist
Review of Particle Physics 2012 (to appear)

5. **The $\eta(1405)$, $\eta(1475)$, $f_1(1420)$, and $f_1(1510)$**
C. Amsler and A. Masoni
Review of Particle Physics 2012 (to appear)

6. **Quark Model**
C. Amsler, T. DeGrand and B. Krusche
Review of Particle Physics 2012 (to appear)

7. Centrality dependence of dihadron correlations and azimuthal anisotropy harmonics in PbPb collisions at $\sqrt{s_{NN}} = 2.76$ TeV
CMS Collaboration
Pre-print: arXiv:1201.3158

8. Suppression of non-prompt J/ψ, prompt J/ψ, and $Y(1S)$ in PbPb collisions at $\sqrt{s_{NN}} = 2.76$ TeV
CMS Collaboration
Pre-print: arXiv:1201.5069

9. Measurement of the inclusive production cross sections for forward jets and for dijet events with one forward and one central jet in pp collisions at $\sqrt{s} = 7$ TeV
CMS Collaboration
Pre-print: arXiv:1202.0704

10. Search for a Higgs boson in the decay channel $H \rightarrow ZZ^{(*)} \rightarrow q\bar{q}l^{-}l^{+}$ in pp collisions at $\sqrt{s} = 7$ TeV
CMS Collaboration
Pre-print: arXiv:1202.1416

11. Search for the standard model Higgs boson decaying into two photons in pp collisions at $\sqrt{s} = 7$ TeV
CMS Collaboration
Pre-print: arXiv:1202.1487

12. Study of high-p_T charged particle suppression in PbPb compared to pp collisions at $\sqrt{s_{NN}} = 2.76$ TeV
CMS Collaboration
Pre-print: arXiv:1202.2554

13. Search for the standard model Higgs boson in the $H \rightarrow ZZ \rightarrow 2l2\nu$ channel in pp collisions at $\sqrt{s} = 7$ TeV
CMS Collaboration
Pre-print: arXiv:1202.3478

14. **Search for the standard model Higgs boson in the $H \rightarrow ZZ \rightarrow l^{+}l^{-}\tau^{+}\tau^{-}$ decay channel in pp collisions at $\sqrt{s} = 7$ TeV**
CMS Collaboration
Pre-print: arXiv:1202.3617

15. Search for large extra dimensions in dimuon and dielectron events in pp collisions at $\sqrt{s} = 7$ TeV
CMS Collaboration
Pre-print: arXiv:1202.3827

16. **Search for neutral Higgs bosons decaying to tau pairs in pp collisions at $\sqrt{s} = 7$ TeV**
CMS Collaboration
Pre-print: arXiv:1202.4083

17. **Inclusive b-jet production in pp collisions at $\sqrt{s} = 7$ TeV**
CMS Collaboration
Pre-print: arXiv:1202.4617

18. Jet momentum dependence of jet quenching in PbPb collisions at $\sqrt{s_{NN}} = 2.76$ TeV
CMS Collaboration
Pre-print: arXiv:1202.5022

19. Search for quark compositeness in dijet angular distributions from pp collisions at $\sqrt{s} = 7$ TeV
CMS Collaboration
Pre-print: arXiv:1202.5535

20. Search for microscopic black holes in pp collisions at $\sqrt{s} = 7$ TeV
    CMS Collaboration
    Pre-print: arXiv:1202.6396

21. **Measurement of the cross section for production of $pp \to b\bar{b}X$, decaying to muons in pp collisions at $\sqrt{s} = 7$ TeV**
    CMS Collaboration
    Pre-print: arXiv:1203.3458

22. **Search for $B_s \to \mu^+\mu^-$ and $B^0 \to \mu^+\mu^-$ decays**
    CMS Collaboration
    Pre-print: arXiv:1203.3976

23. Search for heavy, top-like quark pair production in the dilepton final state in pp collisions at $\sqrt{s} = 7$ TeV
    CMS Collaboration
    Pre-print: CERN-PH-EP-2012-081

Reports

1. **Angular correlation between B-hadrons produced in association with a Z-boson in pp collisions at $\sqrt{s}$ = 7 TeV**
   S. de Visscher, C. Favaro, V. Chiochia, A. Schmidt, C. Amsler, P. Bortignon, C. Grab, A. Rizzi
   CMS PAS EWK-11-015

2. **Observation of a new Ξ_b-baryon**
   E. Aguiló
   CMS PAS BPH-12-001

Lectures

1. E. Aguiló
   13th International Conference on B-Physics at Hadron Machines (Beauty2011), Amsterdam, The Netherlands
   5 April 2011
   "Measurement of exclusive b-hadron production at 7 TeV with the CMS experiment"

2. E. Aguiló
   Seminar, Laboratoire de Physique des Hautes Energies, EPFL, Lausanne, Switzerland
   31 October 2011
   "Recent results from proton-proton collisions at CMS"

   E. Aguiló
   Rencontres de Moriond on QCD and High Energy Interactions, La Thuile, Italy
   12 March 2012
   "Heavy Flavour Production at E_{cm} = 7 TeV"

3. V. Chiochia:
   Seminar on Particle Physics, Physikalisches Institut, Bonn, Germany
   19 May 2011
   "Recent heavy flavor measurements at CMS"

4. V. Chiochia
   Workshop on Implications of LHC results for TeV-scale physics, CERN, Geneva, Switzerland
   29 August 2011
   ”BSM flavour physics signatures from ATLAS and CMS”

5. V. Chiochia
   PH Colloquium, CERN, Geneva, Switzerland
   11 October 2011
   “Heavy Flavor physics with the CMS experiment”

6. V.Chiochia
   Seminar, INFN Pisa, Italy
   25 October 2011
   “Heavy flavour physics with the CMS experiment”

7. V. Chiochia
   Hadron Collider Physics Symposium 2011 (HCP 2011), Paris, France
   17 November 2011
   ”Heavy flavor physics with the CMS experiment”

8. V. Chiochia
   Workshop on New Physics from Heavy Quarks at Hadron Colliders, University of Washington, Seattle, USA
   7 February 2012
   ”Measurements of b-quark production with the CMS experiment”

9. C. Favaro
   Students LHCC poster session, CERN, Geneva, Switzerland
   21 March 2012
   ”Angular correlation between B-hadrons produced in association with a Z-boson”

10. P. Otyugova
    Physics at LHC 2011 Conference (PLHC2011), Perugia, Italy
    6 June 2011
    “Measurements of B- production with the CMS experiment”

11. C. Regenfus
    12th Int. Conf. on Topics in Astroparticle and Underground Physics (TAUP 2011), Munich, Germany
    8 September 2011
    “Study of nuclear recoils in liquid argon”

12. A. Schmidt
    XIX International Workshop on Deep-Inelastic Scattering and Related Subjects (DIS 2011), Newport News, USA
    11 April 2011
    “Measurements of inclusive b-quark production with CMS”

13. H. Snoek:
    13th International Conference on B-Physics at Hadron Machines (Beauty2011), Amsterdam, The Netherlands

4 April 2011
"CMS detector performance"

14. J. Storey
10th international conference on Low Energy Antiproton Physics (LEAP 11), Vancouver, Canada
29 April 2011
"Towards the production of an ultra cold antihydrogen beam with the AEgIS apparatus"

15. J. Storey
Colloquium, Laboratoire Leprince-Ringuet, Palaiseau, France
16 May 2011
"AEgIS : Measuring the fall of antihydrogen (with a detour through antihydrogen physics)"

16. S. de Visscher
Phenomenology Symposium, Univ. Wisconsin at Madison, USA
9 May 2011
"Recent heavy flavor results from CMS "

17. M. Verzetti
Swiss Physical Society, EPFL, Lausanne, Switzerland
15 June 2011
"Search for MSSM Higgs decay into tau pairs with the CMS experiment"

18. M. Verzetti
International Europhysics Conferencence on High Energy Physics (EPS 2011), Grenoble, France
21 July 2011
"Tau identification at CMS"

AEgIS Collaboration (2012):
INFN Bescia - Firenze - Genova - Milano - Padova - Pavia - Trento, CERN, MPI-K (Heidelberg), Kirchoff Inst. of Phys (Heidelberg), INR (Moscow), ITEP (Moscow), Univ. Claude Bernard (Lyon), Univ. of Oslo, Univ. of Bergen, Czech Tech. Univ (Prague), ETH-Zurich, Politecnico Milano, Laboratoire Aimé Cotton (Orsay), Univ. of Zurich.

ArDM Collaboration (2010):
C. Amsler, A. Badertscher, V. Boccone, A. Bueno, M.C. Carmona-Benitez, W. Creus, A. Curioni, M. Daniel, E. J. Dawe, U. Degunda, A. Gendotti, L. Epprecht, S. Horikawa, L. Kaufmann, L. Knecht, M. Laffranchi, C. Lazzaro, P. K. Lightfoot, D. Lussi, J. Lozano, A. Marchionni, K. Mavrokoridis, A. Melgarejo, P. Mijakowski, G. Natterer, S. Navas-Concha, P. Otyugova, M. de Prado, P. Przewlocki, C. Regenfus, F. Resnati, M. Robinson, J. Rochet, L. Romero, E. Rondio, A. Rubbia, L. Scotto-Lavina, N.J.C. Spooner, T. Strauss, J. Ulbricht, and T. Viant.

CMS Collaboration (2012):
see http://greybook.cern.ch/programmes/experiments/CMS.html

DARWIN Collaboration (2012):
Subatech (France), University of Münster, MPIK Heidelberg, University of Karlsruhe, University of Mainz, TU-Dresden, INFN (LNGS - Torino - Napoli - Padova - Pavia - Perugia - Milano - Bologna), Weizmann, NIKHEF, University of Zurich, ETH-Zurich, Columbia University, Princeton University, UCLA, Arizona State University.

DIRAC Collaboration (2012):
Bern University, CERN, CIEMAT (Madrid), Czech Technical University, IHEP Protvino, National Institute for Physics and Nuclear Engineering (Bucharest), INFN - Frascati - Messina - Trieste, Institute of Physics ASCR (Prague), Ioannina University, JINR (Dubna), KEK, Kyoto Sangyo University, Moscow State University, Nuclear Physics Institute (Rez), Tokyo Metropolitan University, Universités Paris VI/VII, UOEH-Kyushu, Wisconsin University, Zurich University.

PARTICLE DATA Group (2010):
K. Nakamura, K. Hagiwara, K. Hikasa, H. Murayama, M. Tanabashi, T. Watari, C. Amsler, M. Antonelli, D. M. Asner, H. Baer, H. R. Band, R. M. Barnett, T. Basaglia, E. Bergren, J. Beringer, G. Bernardi, W. Bertl, H. Bichsel, O. Biebel, E. Blucher, S. Blusk, R. N. Cahn, M. Carena, A. Ceccucci, D. Chakraborty, M. -C. Chen, R. S. Chivukula, G. Cowan, O. Dahl, G. D'Ambrosio, T. Damour, D. de Florian, A. de Gouvea, T. DeGrand, G. Dissertori, B. Dobrescu, M. Doser, M. Drees, D. A. Edwards, S. Eidelman, J. Erler, V. V. Ezhela, W. Fetscher, B. D. Fields, B. Foster, T. K. Gaisser, L. Garren, H. -J. Gerber, G. Gerbier, T. Gherghetta, G. F. Giudice, S. Golwala, M. Goodman, C. Grab, A. V. Gritsan, J. -F. Grivaz, D. E. Groom, M. Grnewald, A. Gurtu, , T. Gutsche, H. E. Haber, C. Hagmann, K. G. Hayes, M. Heffner, B. Heltsley, J. J. Hernndez-Rey, A. Höcker, J. Holder, J. Huston, J. D. Jackson, K. F. Johnson, T. Junk, A. Karle, D. Karlen, B. Kayser, D. Kirkby, S. R. Klein, C. Kolda, R. V. Kowalewski, B. Krusche, Yu. V. Kuyanov, Y. Kwon, O. Lahav, P. Langacker, A. Liddle, Z. Ligeti, C. -J. Lin, T. M. Liss, L. Littenberg, K. S. Lugovsky, S. B. Lugovsky, J. Lys, H. Mahlke, T. Mannel, A. V. Manohar, W. J. Marciano, A. D. Martin, A. Masoni, D. Milstead, R. Miquel, K. Mnig, M. Narain, P. Nason, S. Navas, P. Nevski, Y. Nir, K. A. Olive, L. Pape, C. Patrignani, J. A. Peacock, S. T. Petcov, A. Piepke, G. Punzi, A. Quadt, , S. Raby, G. Raffelt, B. N. Ratcliff, P. Richardson, S. Roesler, S. Rolli, A. Romaniouk, L. J. Rosenberg, J. L. Rosner, C. T. Sachrajda, Y. Sakai, G. P. Salam, S. Sarkar, F. Sauli, O. Schneider, K. Scholberg, D. Scott, W. G. Seligman, M. H. Shaevitz, M. Silari, T. Sjstrand, J. G. Smith, G. F. Smoot, S. Spanier, H. Spieler, A. Stahl, T. Stanev, S. L. Stone, T. Sumiyoshi, M. J. Syphers, J. Terning, M. Titov, N. P. Tkachenko, N. A. Trnqvist, D. Tovey, T. G. Trippe, G. Valencia, K. van Bibber, G. Venanzoni, M. G. Vincter, P. Vogel, A. Vogt, W. Walkowiak, C. W. Walter, D. R. Ward, B. R. Webber, G. Weiglein, E. J. Weinberg, J. D. Wells, A. Wheeler, L. R. Wiencke, C. G. Wohl, L. Wolfenstein, J. Womersley, C. L. Woody, R. L. Workman, A. Yamamoto, W. -M. Yao, O. V. Zenin, J. Zhang, R. -Y. Zhu, P. A. Zyla.